

University at Albany, State University of New York

## Scholars Archive

---

Nanoscale Science & Engineering (discontinued  
with class year 2014)

Honors College

---

5-2016

# Modeling Secondary Electron Trajectories in Scanning Electron Microscopes

Kevin McNamara

*University at Albany, State University of New York*

Joshua Miller

*University at Albany, State University of New York*

Follow this and additional works at: [https://scholarsarchive.library.albany.edu/honorscollege\\_nano](https://scholarsarchive.library.albany.edu/honorscollege_nano)



Part of the [Nanoscience and Nanotechnology Commons](#)

---

### Recommended Citation

McNamara, Kevin and Miller, Joshua, "Modeling Secondary Electron Trajectories in Scanning Electron Microscopes" (2016). *Nanoscale Science & Engineering (discontinued with class year 2014)*. 17.  
[https://scholarsarchive.library.albany.edu/honorscollege\\_nano/17](https://scholarsarchive.library.albany.edu/honorscollege_nano/17)

This Honors Thesis is brought to you for free and open access by the Honors College at Scholars Archive. It has been accepted for inclusion in Nanoscale Science & Engineering (discontinued with class year 2014) by an authorized administrator of Scholars Archive. For more information, please contact [scholarsarchive@albany.edu](mailto:scholarsarchive@albany.edu).

# MODELING SECONDARY ELECTRON TRAJECTORIES IN SCANNING ELECTRON MICROSCOPES

By: Kevin McNamara and Joshua Miller

An honors thesis presented to the  
College of Nanoscale Science and Engineering  
University at Albany, State University of New York  
in partial fulfillment of the requirements  
for graduation from The Honors College.

Research Advisor: Dr. Eric Lifshin

May 2016

## **ACKNOWLEDGEMENTS**

We sincerely thank our research advisor Dr. Eric Lifshin for his guidance on this project. We also acknowledge our other group members: Mark Schaefer, Kevin Reilly, Erik Scheltinga, and Ben Trudell. We express our gratitude to all the developers who contributed to the creation of the two modeling programs used in this work, CASINO and SIMION.

## **ABSTRACT**

The efficiency of secondary electron collection by a scanning electron microscope detector is not generally known, particularly as the electric field on the detector is varied. It is often assumed that the detector collects almost all of the secondary electrons emitted from the sample. This work seeks to better understand the mechanism of secondary electron collection by the detector in order to optimize collection efficiency. The benefit of collecting more secondary electrons is the enhancement of the signal-to-noise ratio, which means better quality images can be obtained, allowing us to better understand the relationship between secondary electron images and the objects they represent.

Secondary electron trajectory modeling was done to evaluate the efficiency of the current SEM detector setup. The CASINO modeling program was used to model the trajectories of secondary electrons generated within the sample to determine the initial directions and energies of the emitted secondary electrons. The SIMION modeling program was used to model the trajectories of secondary electrons emitted from the sample using a uniform distribution of initial directions and energies to determine the collection efficiency of the detector. Certain setup and operating parameters, such as the size of the detector and the potential applied to it, were studied for the optimization of secondary electron collection efficiency. A more efficient detector setup was designed using a pusher electrode to collect more secondary electrons emitted from the sample at high elevation angles. Trajectory modeling using SIMION was done to evaluate the efficiency of our improved system design, validating its performance enhancement. Although a bridge between CASINO and SIMION has not yet been made, useful data was obtained from both CASINO and SIMION simulations.

# TABLE OF CONTENTS

|   |     |
|---|-----|
| ACKNOWLEDGEMENTS.....                                   | ii  |
| ABSTRACT.....   | iii |
| TABLE OF CONTENTS.....                                  | iv  |
| INTRODUCTION.....                                       | 1   |
| Working Principle of Scanning Electron Microscopes..... | 2   |
| Electron-Solid Interactions.....                        | 5   |
| CASINO Modeling Program.....                            | 13  |
| Detection of Emitted Electrons.....                     | 18  |
| SIMION Modeling Program.....                            | 20  |
| RESULTS AND DISCUSSION.....                             | 27  |
| CASINO Data.....  | 28  |
| SIMION Data.....  | 41  |
| Our Improved System Design.....                         | 46  |
| CONCLUSION.....   | 52  |
| FUTURE WORK.....  | 53  |
| REFERENCES.....   | 54  |

## **INTRODUCTION**

An introduction to the working principle of a scanning electron microscope is necessary to understand this research. Furthermore, knowledge of electron-solid interactions is essential to understand the process of secondary electron emission. Background on how the CASINO modeling program simulates electron-solid interactions is presented in this section. An understanding of electron trajectories within an electric field is needed to comprehend the process of secondary electron detection. Background on how the SIMION modeling program simulates electron trajectories is also presented in this section.

## Working Principle of Scanning Electron Microscopes

A scanning electron microscope (SEM) is a type of electron microscope that produces a magnified image of a sample's surface topography by scanning across the sample with a focused beam of electrons. It is used for the characterization of materials on the nanoscale. In addition to seeing nanoscale structures, it can also provide information on chemical composition, crystalline structure, and electrical behavior of the sample surface ( $\sim 1 \mu\text{m}$  depth).<sup>1</sup>

There are several components of an SEM that are crucial to understanding its operation. Figure 1 shows the main components of an SEM.<sup>1</sup> The tool is located inside a chamber that utilizes a pumping system to obtain high vacuum ( $\sim 10^{-6}$  Torr). A vacuum chamber is needed since the beam electrons would scatter with gas molecules in open air. The electron beam, having energy up to 30 keV, is created by an electron gun that emits electrons from a filament. The most common electron gun is the tungsten hairpin filament. The high negative voltage applied to the filament causes it to heat up to the point where electrons gain enough thermal energy to overcome the filament's work function, enabling electrons to be emitted thermionically in all directions. Due to the negative bias of the filament (which acts like a cathode), the emitted electrons are accelerated down through the opening in a positively biased anode aperture plate in the direction of the grounded sample at the bottom of the column.<sup>2</sup>

As the electrons travel down the column, magnetic lenses demagnify the electron beam: a condenser lens controls the diameter of the beam and an objective lens focuses the beam onto the sample. The diameter of the electron beam on the sample (called the probe size) can be as small as 1 nm. At the end of the column, the beam passes through deflection coils that scan the beam in

a raster pattern over a rectangular area of the sample surface. The final component in the column is an aperture that limits the area through which the electron beam can reach the sample.<sup>2</sup>

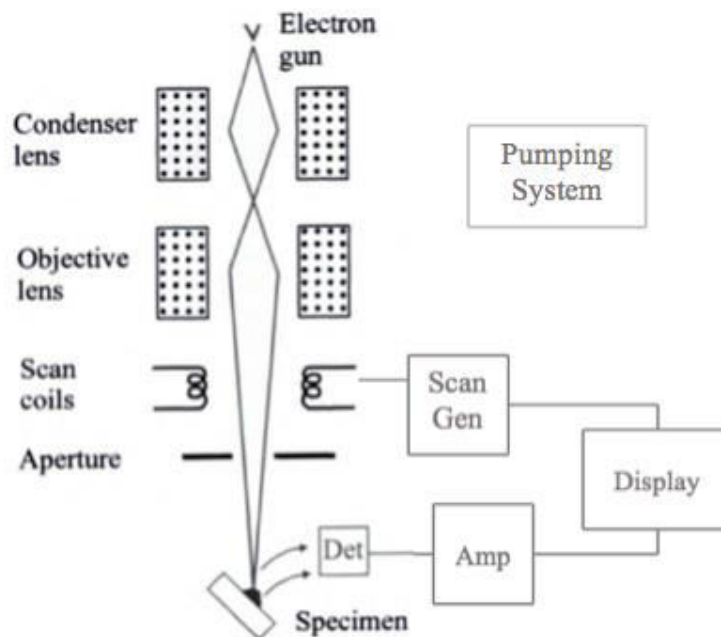


Figure 1: The main components of an SEM.

As the electron beam scans over the entirety of the sample, the beam electrons interact with the atoms near the surface of the sample (see “Electron-Solid Interactions” section), producing various signals such as the emission of backscattered and secondary electrons. A specialized electron detector (see “Detection of Emitted Electrons” section) collects a particular electron signal (either backscattered or secondary electrons) and an amplifier intensifies the signal and then converts it into a grayscale intensity to produce a digital image of the sample. The image (called a micrograph) is displayed on a computer screen. A scan generator synchronizes the position of the electron beam on the sample with its corresponding position on the display, allowing the user to view the image on the display as the sample is being scanned.<sup>2</sup>



The magnification of an SEM is the ratio of the size of the scan on the display to the size of the scan on the sample. Assuming the display screen has a fixed size, higher magnification results from reducing the size of the raster scan on the sample. Magnification values typically range from 10X to 300,000X.<sup>3</sup>

Figure 2 shows an SEM micrograph.<sup>4</sup> Due to the very narrow electron beam, SEM images have a large depth of field, which gives rise to the three-dimensional appearance of the sample's surface structure that can be observed in SEM micrographs. The spatial resolution of an SEM depends on the electron probe size, which itself depends on the de Broglie wavelength of the electrons and the electron-optical system that creates the probe on the sample. The resolution is also limited by the size of the interaction volume (see "Electron-Solid Interactions" section) and the volume of the sample material that interacts with the electron beam. For the best instruments, resolution is typically 2-5 nm.<sup>3</sup>

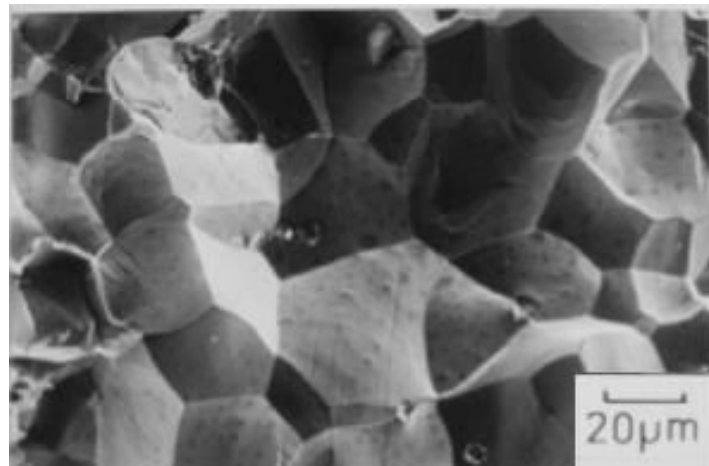


Figure 2: An SEM micrograph.

## Electron-Solid Interactions

Primary electrons (PE) are electrons within the incident beam that have not yet interacted with the sample. The energy exchange between the primary electrons and the sample produces various signals, including the emission of backscattered electrons, secondary electrons, Auger electrons, and electromagnetic radiation. Figure 3 shows the signals emitted from the sample in an SEM.<sup>1</sup> Specialized detectors can detect each of the signals, however, this work focuses on the detection of secondary electrons.

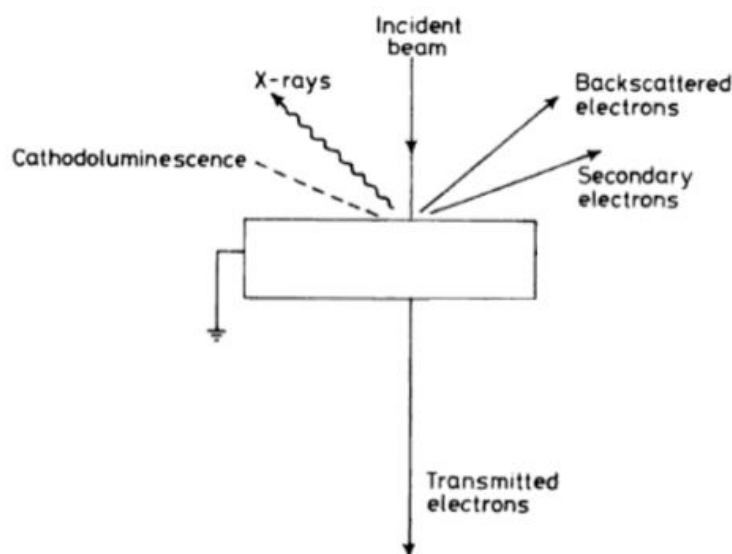


Figure 3: The signals emitted from the sample in an SEM.

When the electron beam interacts with a sample, the primary electrons lose energy by repeated, random inelastic scattering with the sample's atoms (called electronic stopping) within a teardrop-shaped volume of the sample known as the interaction volume. Figure 4 shows the interaction volume in a sample.<sup>1</sup> The consequence of electronic stopping is that the primary electrons have a finite range in the sample called the penetration depth that is on the order of

nanometers to microns depending on the beam's energy and incidence angle as well as the sample's atomic mass. The penetration depth (as well as the interaction volume) increases for higher energy beams and samples with lower atomic masses.<sup>3</sup> This results from the fact that higher energy primary electrons have more available energy to be lost by electronic stopping, which means they can withstand more collisions and thus travel longer distances in the sample, especially in less dense samples.

Different signals have different escape depths, i.e., the maximum distance the signal can travel in the sample and still be emitted. Figure 4 shows the escape depths of the various signals:  $\lambda_{SE}$  is the secondary electron escape depth,  $\lambda_{BE}$  is the backscattered electron escape depth, and  $\lambda_{X-ray}$  is the X-ray escape depth.<sup>3</sup> Depending on various factors such as the beam energy and the sample's atomic mass,  $\lambda_{SE}$  is typically 5–50 nm, while  $\lambda_{BE}$  is typically 0.5–2  $\mu\text{m}$  and  $\lambda_{X-ray}$  is typically 2–10  $\mu\text{m}$ .<sup>4</sup>

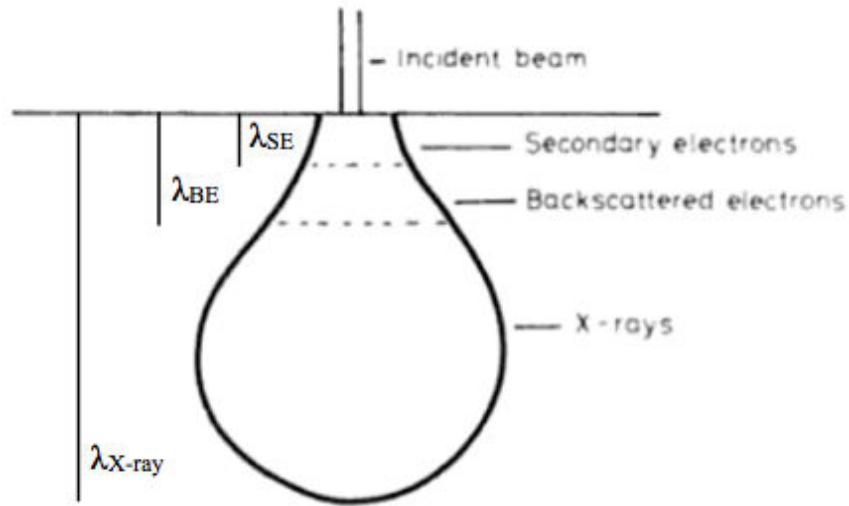


Figure 4: The interaction volume in a sample.

Backscattered electrons (BE) are high-energy electrons ( $> 50$  eV, up to the beam energy) originating from the electron beam that have interacted elastically with the sample's nucleus, causing them to be scattered back in the direction of the incident beam with only a small loss in energy. Figure 5(a) shows an elastic collision of a primary electron with an atom's nucleus resulting in a backscattered electron.<sup>2</sup> Since backscattered electrons have high energy, they can emerge from deeper locations within the sample. The majority of backscattered electrons retain at least 50% of the incident beam energy. The amount of energy a backscattered electron retains upon emission depends on the number of collisions it participated in within the sample (which is a random process) and the energy loss per collision.<sup>4</sup>

Secondary electrons (SE) are low-energy electrons ( $< 50$  eV, peak distribution of 2-5 eV) emitted from the sample's atoms due to the inelastic interaction of the high-energy electron beam with the bound electrons of the sample's atoms. Figure 5(b) shows an inelastic collision of a primary electron with an atom's K-shell electron causing the emission of a secondary electron.<sup>2</sup> Since secondary electrons have low energy, they can only escape from the sample if generated very close to the sample surface ( $< 5$  nm for conductors,  $< 50$  nm for insulators), thus providing information about surface morphology.<sup>4</sup> For an insulator, the escape depth is greater than for a metal because a particle in a metal has a shorter mean free path due to the metal's sea of free valence electrons.

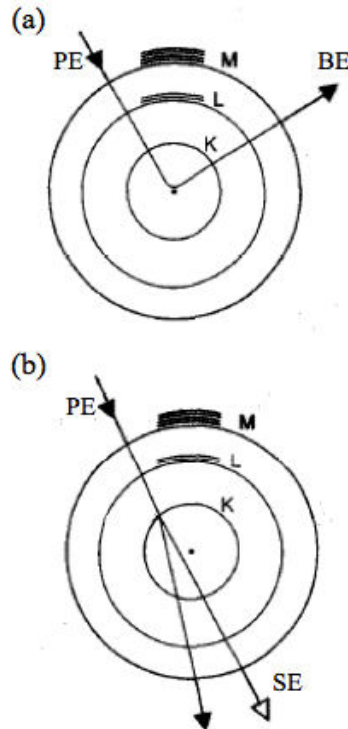


Figure 5: (a) Elastic collision of a primary electron with an atom's nucleus resulting in a backscattered electron. (b) Inelastic collision of a primary electron with an atom's K-shell electron causing the emission of a secondary electron.

Secondary electrons are classified into three types: SE(1) are secondary electrons released by incident primary electrons, SE(2) are secondary electrons released by exiting backscattered electrons, and SE(3) are secondary electrons released by backscattered electrons striking objects in the chamber. Figure 6 shows the three types of secondary electron signals in an SEM.<sup>5</sup> Note in Figure 6 the presence of a contamination layer C at the surface. SE(1) are generated very close to the incident beam and so they produce a signal at the point of interest on the sample, resulting in high spatial resolution. SE(II) are generated farther away from the incident beam and thus lower the spatial resolution of the total signal. SE(3) do not provide information about sample surface morphology and so they also lower the spatial resolution.<sup>4</sup>

Figure 7 shows the spatial distribution of secondary electron emission.<sup>1</sup> The intensity of secondary electron emission vs. the distance from the incident beam follows a cosine distribution. This intensity profile results from the fact that many SE(1) are generated near the incident beam and few SE(2) are generated at distances far away from the incident beam.

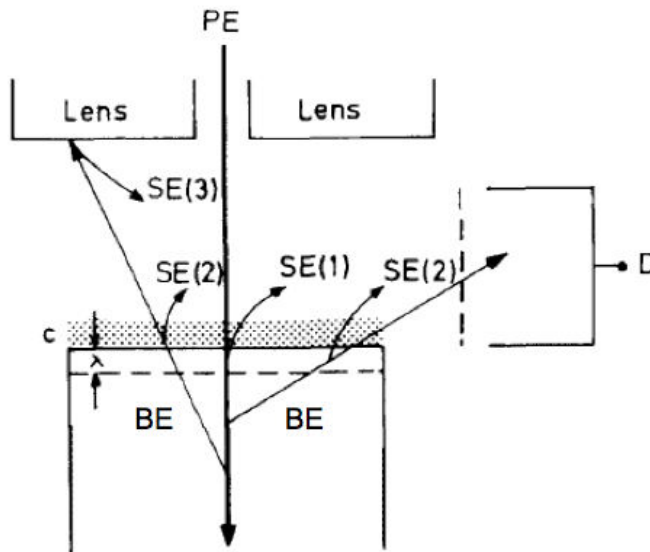


Figure 6: Three types of secondary electron signals in an SEM.

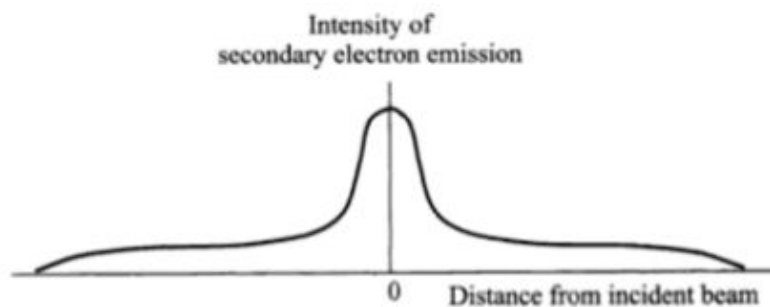


Figure 7: The spatial distribution of secondary electron emission.

The numbers of secondary and backscattered electrons emitted from the sample for each incident electron are known as the secondary electron coefficient/yield ( $\delta$ ) and the backscattered electron coefficient/yield ( $\eta$ ), respectively. Figure 8 shows the effect of atomic number on electron yield:  $\eta$  is strongly dependent on the atomic number of the sample whereas  $\delta$  is not.<sup>1</sup> Elements that have a high atomic number produce more backscattered electrons than ones that have a low atomic number. As shown in Figure 8,  $\eta$  begins to level off at 0.5 for elements with an atomic number greater than gold ( $Z = 79$ ). Elements that have a high atomic number also produce slightly more secondary electrons than ones that have a low atomic number. As shown in Figure 8,  $\delta$  is around 0.1 for all elements, but it increases slightly with increasing atomic number. This is mainly attributed to the increase in SE(2) since many more backscattered electrons are produced for elements with higher atomic numbers and so more SE(2) are also generated.<sup>4</sup>

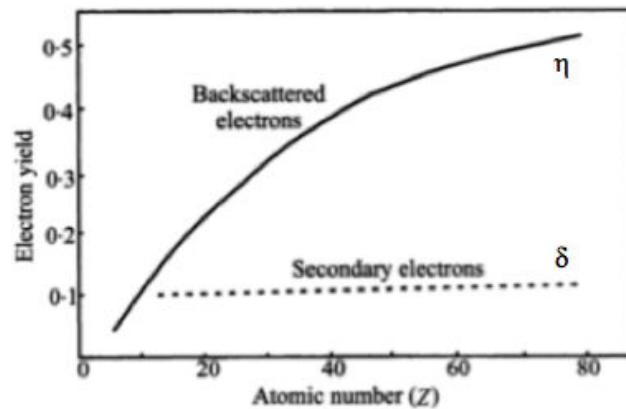


Figure 8: The effect of atomic number on electron yield.

The secondary electron yield  $\delta$  depends strongly on the electron beam energy. At lower beam energies, the secondary electrons are generated closer to the sample surface and thus they have a higher escape probability. At higher beam energies, the number of secondary electrons

generated increases, but they are generated deeper in the sample and thus their escape probability decreases significantly. The secondary electron yield also depends on the sample tilt. Figure 9 shows the effect of sample tilt on secondary electron yield.<sup>5</sup> Inclined surfaces (or tilted samples) produce greater secondary electron yield. This occurs because when the sample is tilted to some angle relative to the primary electron beam, a greater number of secondary electrons are produced within the escape region due to the larger path length of the beam within the escape region. The greater the tilt angle, the greater the secondary electron yield. In an SEM, when detecting secondary electrons, the sample is inclined at an angle relative to the electron beam in order to produce a greater signal.

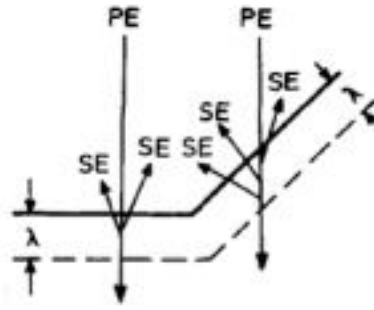


Figure 9: The effect of sample tilt on secondary electron yield.

Different secondary electron yields of adjacent surface objects lead to contrast between their corresponding pixels in SEM micrographs. Contrast, which is a measure of the difference in intensity of object elements A and B divided by the sum of their intensities, is given by

$$C = \frac{I_A - I_B}{I_A + I_B} = \frac{I}{2\bar{I}} \quad (1)$$

where  $I = I_A - I_B$  and  $\bar{I} = \frac{I_A + I_B}{2}$ . There are two main types of contrast in an SEM:

topography contrast and material contrast. Topography contrast arises from point-to-point



changes in the electron yield due to different inclinations of surface details. The greater the difference in secondary electron yields of adjacent surface objects, the greater the contrast and thus large inclinations and steep edges appear very bright in SEM micrographs. Topography contrast is less apparent for backscattered electrons. There is also material contrast (or Z contrast), which arises from point-to-point changes in the electron yield due to the different materials at the surface, but this effect is small for secondary electrons. Material contrast is much more apparent for backscattered electrons.<sup>4</sup>

The quality of an image produced by an SEM depends strongly on the signal-to-noise ratio (S/N). Signal generation is a stochastic process that follows a Poisson distribution, for which the standard deviation of the signal ( $\sigma$ ) is equal to the square root of the mean of the signal ( $\bar{s}$ ). S/N is given by

$$\frac{S}{N} = \frac{\bar{s}}{\sqrt{\bar{s}}} = \sqrt{\bar{s}} \quad (2)$$

where the signal  $S = \bar{s}$  and the noise  $N = \sqrt{\bar{s}}$ . High quality SEM images require a high S/N.<sup>4</sup>

## CASINO Modeling Program

CASINO (v3.3.0.4) is the first modeling program that was used for the simulations in this work. It is a 3D version that is an update from the 2D version, which has been used in many research studies to date.<sup>6</sup> The program uses a Monte Carlo method to calculate electron trajectories within the sample. This method uses random numbers and probability distributions to represent the physical interactions between the electrons and the sample.

The electron trajectory is represented by separate elastic scattering events while the inelastic events are approximated by the mean energy loss model between two elastic scattering events. The final calculation of each electron trajectory can be described by the following steps. First, the initial position and energy of the electron are calculated from user specified beam parameters. Examples of the parameters that can be varied will be discussed later in this section. From this initial position, the electron will impinge on the sample. The distance between two collisions is obtained based on the total elastic cross-section in which a random number is used to distribute the distance following a probability distribution. The elastic scattering angle  $\theta$  is then determined from another random number and using the differential cross-section that was calculated or by just using standardized tabulated values. When the electron intercepts a triangle (used to describe the sample), the segment is terminated at the boundary and a new segment is generated randomly from the properties of the new region. Electron transport is thought to be a Markov process. This means that past events do not affect future events. These steps are then repeated until an electron leaves the sample or is trapped inside the sample.<sup>7</sup>

If secondary electrons are simulated, the region work function is used as a threshold value. CASINO is able to keep track of the coordinate when a change of region event occurs

during the simulation of the electron trajectory. Tabulated values from the ELSEPA cross-section program are used in CASINO. These calculated values are included in CASINO to allow for accurate simulations of electron scattering. The energy grid used in the tabulated data for each element was chosen in order to give an interpolation error of less than one percent so long as linear interpolation is used.<sup>7</sup>

The 3D version of CASINO added a feature that allows secondary electrons to be simulated along with the calculation of secondary electron yields. The fast secondary electrons use the Moller equation while the slow secondary electrons are generated from plasmon theory. The work function and plasmon energies are the two parameters needed to generate secondary electrons in a region. CASINO automatically puts in these parameters for the element selected, but the user can change these values if need be.

The CASINO program allows the user to choose several varying properties of the microscope to be used in the simulation. Also, simulation properties can be changed. Since many properties of the microscope can greatly affect the simulation time or the amount of computer memory needed to carry out the simulation, the program allows multiple cores to be used to make the simulations faster and less stringent on the memory of the computer. If one wants to make a simulation faster or less harsh on computer memory, many properties can be deactivated to allow for quicker simulations. In order to better explain all of the functions of the program, Figure 10 will be referred to. The grid that takes up most of the left half of the setup menu shows the sample that the user will simulate. Pictured here is a simple square substrate. The grid also shows the dimensions of the object in nanometers. Since this is a 3D program, the user can even rotate and view the object in 3D in this view if desired. Under the grid, there is a section that is labeled “Mouse Pointer Properties.” It is here where the user can add as many points they want

for the simulation. This can be done simply by clicking on the sample to create a point, or by actually entering the values in the box and simply clicking the “Add Point” button. The more points that the user wants to simulate, the more time and memory the simulation will need to run. To the right of the grid, the user has the choice to change several different parameters of the microscope. The first property is the number of simulated electrons. One of the main focus areas of our simulations was to determine the ideal or minimum number of electrons needed in order to get significant statistical data. In this area, the user can also change the beam energy and can choose to conserve the data for each simulated point that was selected; however, if one wants faster simulations, it is best to leave this box unchecked.

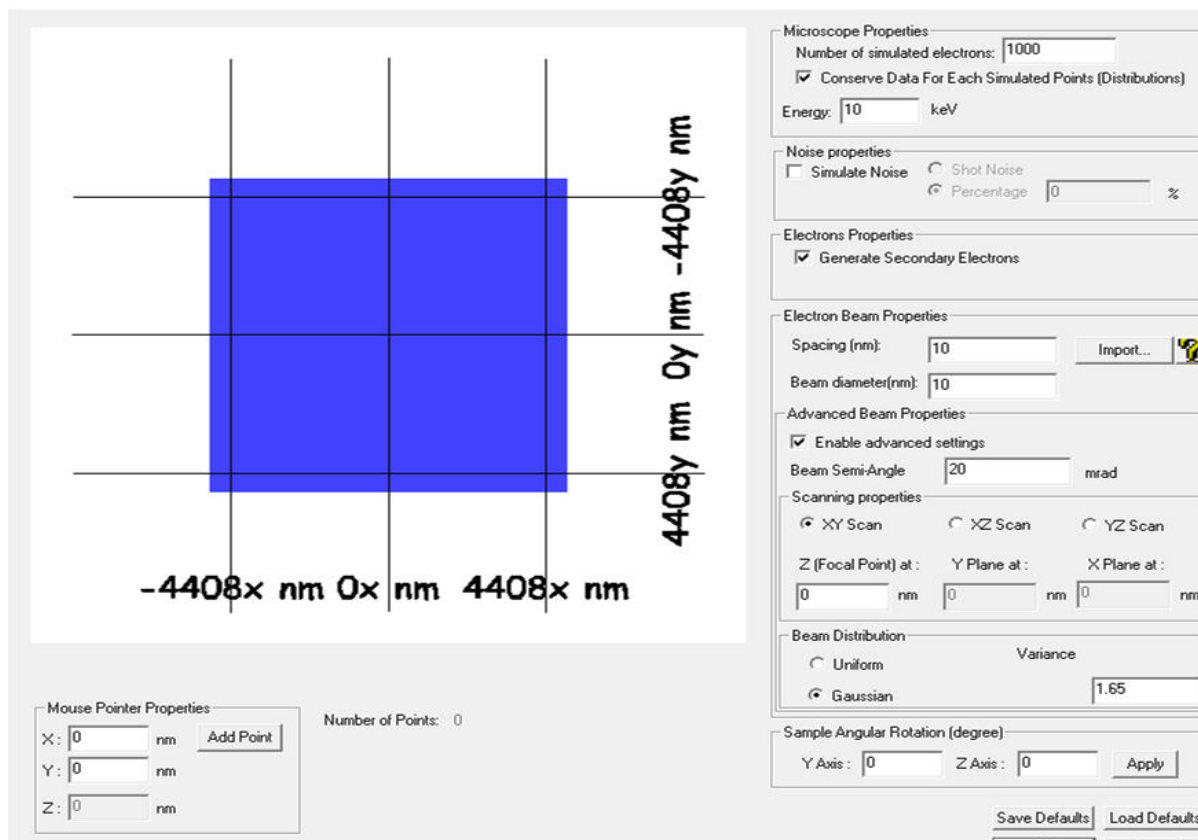


Figure 10: CASINO setup menu.

Moving on, the user can then choose to simulate noise and generate secondary electrons. The secondary electron feature results in a simulation that take much longer; thus, if one is only interested in backscattered electrons, it is best to leave this box unchecked. Under this, the user can actually choose the spacing and diameter of the electron beam. In addition, the user can then choose whether or not to make the beam have a semi-angle. The final set of boxes on the bottom right allow the user to change scanning properties when doing a simulation using multiple points. The raster scan can be done along several different axes. Finally, the user can decide whether to have a beam with a uniform or Gaussian distribution. When clicking the ok dialog box, the program will then ask the user if Monsol settings are appropriate. After simply selecting yes, the program will automatically start the scan on the sample.

Once the scan is complete, the monitor will show a final screen similar to that seen in Figure 11. In Figure 11, the box is a simple gold substrate. The red lines coming out of the sample represent the high energy backscattered electrons while the blue and green lines represent low energy backscattered electrons and secondary electrons, respectively. If the user chose to conserve the data for each simulated point, then graphs of escape depth, energy of emitted backscattered electrons, angular distribution, and many others will be created to allow the user to analyze data on the backscattered electrons. Unfortunately, this type of data cannot be obtained for the secondary electrons in this program. However, data on secondary yields and intensity versus position are created during the simulation.

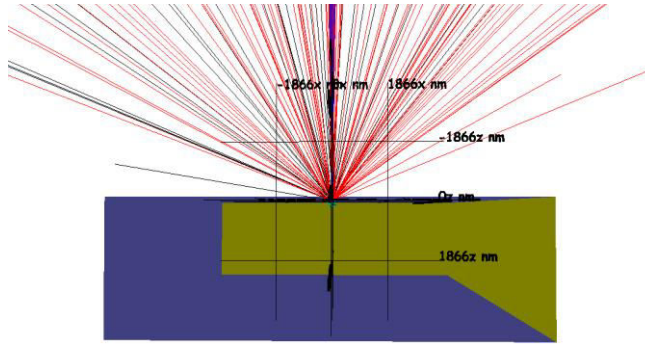


Figure 11: CASINO simulation showing emitted backscattered and secondary electrons.

Figure 12 shows a zoomed in picture of Figure 11 in which the user can now see the secondary electrons generated in the interaction volume of the sample. The secondary electrons generated in the interaction volume are colored green. Many of the secondary electrons generated will not have enough energy to escape. The blue color that is seen represents electrons that are absorbed or transmitted through the sample. As shown in figure 12, no electrons are transmitted because the substrate was made very thick. If the user chose to simulate many different points on the sample, then an intensity graph would be created based on secondary electron yield and it would also create an image of what the sample might look like in an SEM.

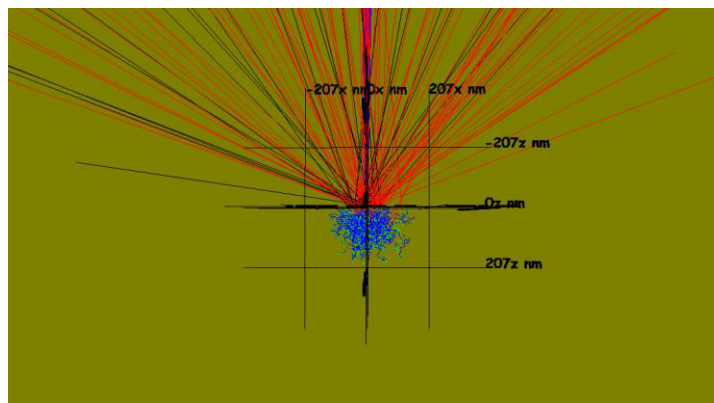


Figure 12: CASINO simulation showing secondary electrons generated in the sample.

## Detection of Emitted Electrons

The most common method of detecting secondary electrons is by using an Everhart-Thornley detector (Figure 13), which consists of an electrically biased control grid, scintillator, light guide, and photomultiplier tube. Since secondary electrons are emitted in various directions from the sample, a small positive voltage (+200 V) is applied to the control grid in order to direct the low-energy, negatively charged secondary electrons towards the detector. This small positive voltage is not strong enough to attract high-energy backscattered electrons. The collected secondary electrons pass through the openings in the control grid towards the scintillator. Since the scintillator has a potential of +10 kV, the secondary electrons are accelerated towards it before striking its metal coating to produce photons through cathodoluminescence. The photons are guided to the photomultiplier via a light pipe.<sup>1</sup>

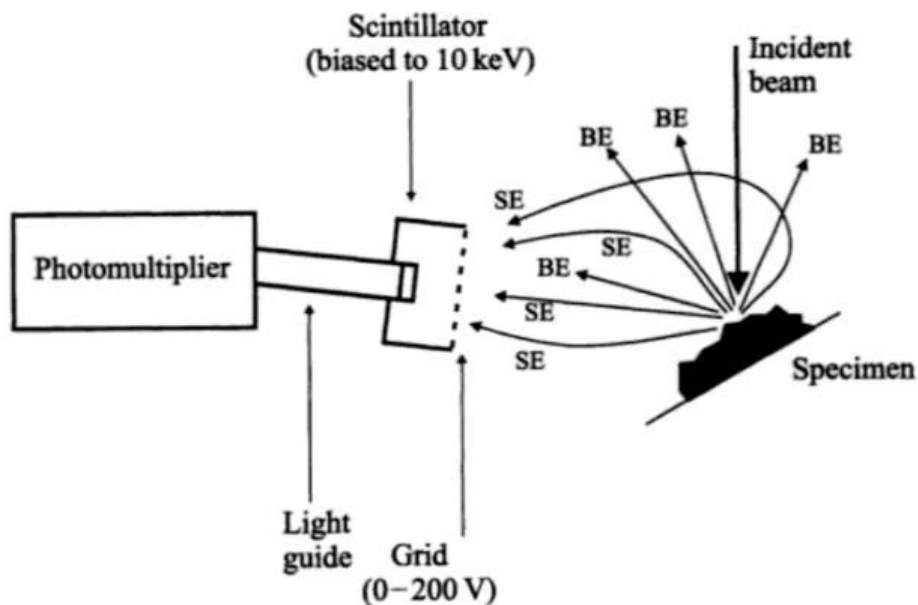


Figure 13: An Everhart-Thornley detector.

When the photons reach the photomultiplier (Figure 14), they strike the photocathode, which causes the emission of photoelectrons by the photoelectric effect. The photoelectrons are multiplied by striking a dynode, which causes secondary electron emission. A chain of dynodes consisting of successive dynodes with increasing positive potential is used to amplify the signal further. Each successive dynode attracts and accelerates the secondary electrons emitted from the prior dynode in order to enhance its own emission of secondary electrons. A voltage divider is used to create the varying potentials of the dynodes. At the end of the tube, the amplified electrical signal reaches the anode and then is converted into a grayscale intensity. It is displayed as a two-dimensional intensity map on a computer screen.<sup>3</sup>

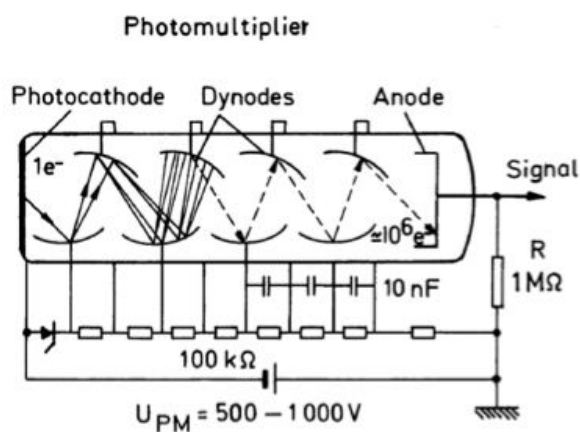


Figure 14: A photomultiplier tube.

The Everhart-Thornley detector, which is positioned to one side of the sample, can also detect backscattered electrons by applying a small negative voltage ( $-100 \text{ V}$ ) to the control grid. This small negative voltage repels low-energy secondary electrons while not affecting the high-energy backscattered electrons. However, this detector is inefficient for the collection of backscattered electrons because it only detects the few backscattered electrons that are emitted in the line of sight of the detector.<sup>1</sup>



## SIMION Modeling Program

SIMION 8.1 is the second modeling program that was used for the simulations in this work. The program simulates the trajectories of charged particles in electric fields under designated electrode configurations when given the initial conditions of the particles. It was used to model the trajectories of secondary electrons emitted from the sample using a uniform distribution of initial directions and energies to determine the collection efficiency of the detector.

On the SIMION main menu (Figure 15), you must first select “New” to create a new potential array. You will be directed to the dimensions setup menu (Figure 16). The program can simulate trajectories for charged particles in electric or magnetic fields, but for this work we only used electric potentials. You must select a particular coordinate system. We used a rectangular coordinate system. You must also choose the number of grid points and the length of the grid unit. We used 1 cm grid units to create a 50 cm x 50 cm array.

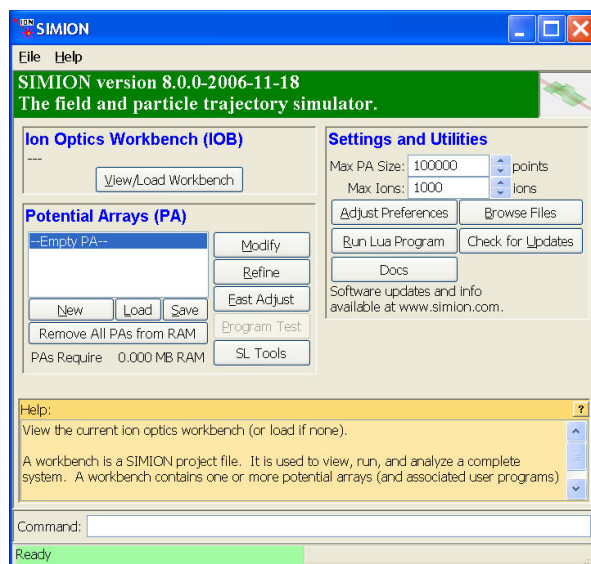


Figure 15: SIMION main menu.

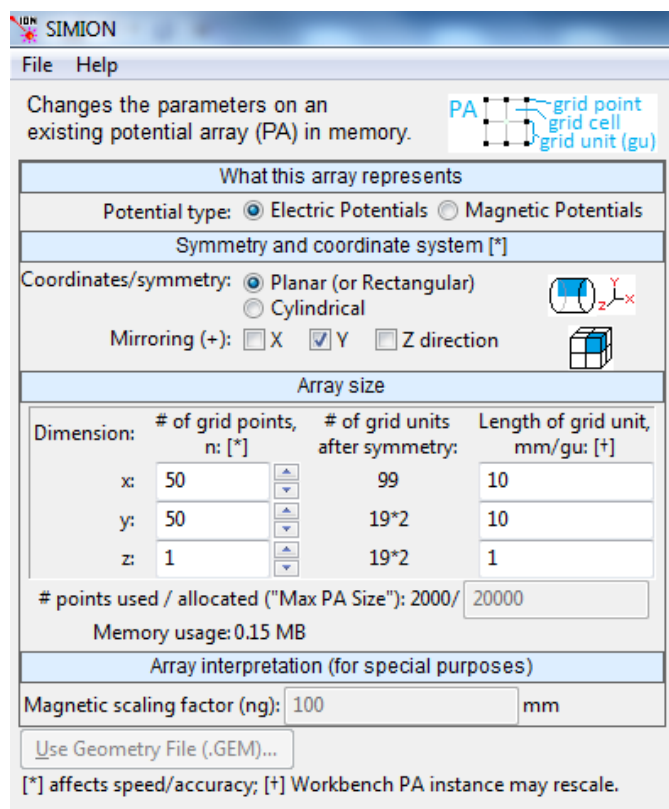


Figure 16: SIMION dimensions setup menu.

After defining the setup dimensions, you must select “Modify” on the main menu screen. You will be directed to the electrode building screen (Figure 17). A potential array with the dimensions you defined will appear in the center of the screen. The array consists of hollow green diamonds that represent non-electrode grid points. You can create electrodes with different shapes such as boxes, lines, and circles. You must define the potentials of the electrodes. To do this, you first define the potential of the electrode and then select the shape you want to draw. Then, you use the cursor to drag an outline of the size of the shape you want to draw. Finally, you select “Replace” and the electrode will be created as a group of red squares in the size of the shape you defined. We used boxes to create the chamber, lines to create the sample, and a circle to create the detector.

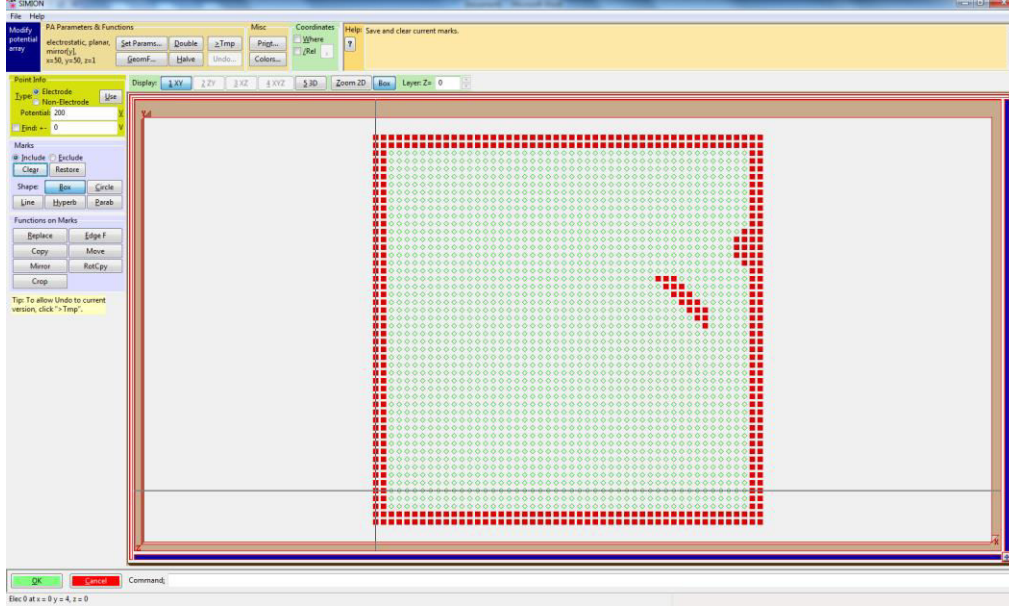


Figure 17: SIMION electrode building screen.

When you are done making your electrode design, you must tell the program to calculate the electric fields for your electrode configuration. You do this by selecting “Refine” on the main menu screen. SIMION calculates a map of the electric field at all points in space by solving Poisson’s equation, which is a differential equation boundary value problem. The theory is as follows: derived from Gauss’s law, we have an expression for the divergence of an electric field

$$\nabla \cdot \vec{E} = \frac{\rho}{\epsilon} \quad (3)$$

where  $\nabla$  is the del operator,  $\vec{E}$  is the electric field,  $\rho$  is the free volumetric charge density, and  $\epsilon$  is the permittivity. Knowing that the electric field is the negative of the potential gradient

$$\vec{E} = -\nabla V \quad (4)$$

where  $V$  is the scalar potential field, we can substitute Equation 4 into Equation 3 to get

$$\nabla^2 V = \frac{\partial^2 V}{\partial x^2} + \frac{\partial^2 V}{\partial y^2} + \frac{\partial^2 V}{\partial z^2} = - \quad (5)$$

where  $\Delta$  is defined in rectangular coordinates. The boundary potentials we defined earlier for the electrodes are needed to solve this three-dimensional 2<sup>nd</sup> order partial differential equation. SIMION uses Equation 5 to first calculate the scalar potential field and then it uses the calculated values for the potential  $V$  to solve Equation 4 for the electric field  $\vec{E}$  at all points on the grid.<sup>3</sup>

After the electric fields are calculated, you can now load the workbench for the model you created. You do this by selecting “View/Load Workbench” on the main menu screen. You will be directed to the workbench where your model will appear in the center of the screen. Figure 18 shows our 2D setup, which imitates the environment inside an SEM: a grounded, square chamber; a grounded, inclined line sample holder; and a semicircular, electrically biased control grid (which acts as the detector). The detector potential can be varied (typically operating at +200–400 V). The typical distances from the sample to the detector in both the x and y directions is between 4–8 cm. The detector size itself is around 4–8 cm in diameter. You do not need to define a sample; instead, you define a point source located just outside the center of the sample holder from which the electrons will emanate. This setup is sufficient to model the trajectories of secondary electrons from the sample holder to the detector.

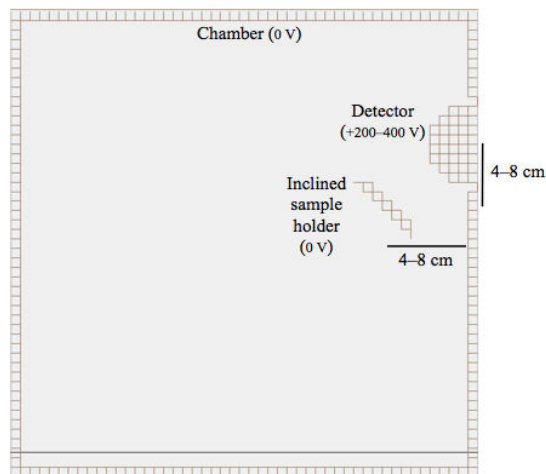


Figure 18: SIMION detector setup.

In order to define the initial conditions of the particles, you must first select the Particles tab at the top of the workbench screen and then select “Define Particles” to open the particle definition screen (Figure 19). You define one particle at a time. You first must select the type of particle. Once you select the particle (e.g. electron), its mass and charge are automatically defined. You need to choose the source position. For this work, we choose the source position to be the point located just outside the center of the sample holder (where the sample would be located). You next have to choose the direction angle. In 2D, you only need to assign an elevation angle, but in 3D you can assign both an elevation angle and an azimuth angle. Lastly, you need to define the kinetic energy of the particle, which is 50 eV or less for secondary electrons.

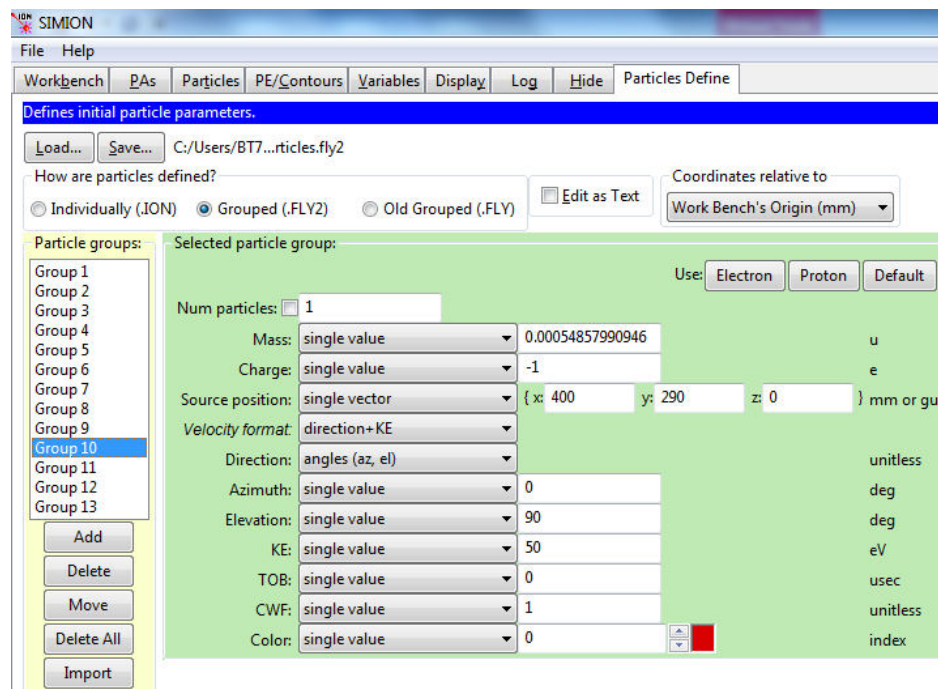


Figure 19: SIMION particle definition screen.

Once the initial conditions of the particles are set, you select “Fly’m” at the bottom left of the workbench screen to simulate the particle trajectories. SIMION calculates particle trajectories in electric fields using the 4<sup>th</sup> order Runge-Kutta method to find an approximate solution to the Lorentz equation, which is a differential equation initial value problem. The theory is as follows: the Lorentz equation is given by

$$\vec{F} = q(\vec{E} + \vec{v} \times \vec{B}) \quad (6)$$

where  $\vec{F}$  is the force,  $q$  is the charge,  $\vec{E}$  is the electric field (calculated before),  $\vec{v}$  is the velocity, and  $\vec{B}$  is the magnetic field. Since there is no magnetic field in our model,  $\vec{B} = \vec{0}$ . Knowing Newton’s 2<sup>nd</sup> law ( $\vec{F} = m\vec{a}$ ), Equation 6 simplifies to

$$\vec{F} = q\vec{E} = m\vec{a} \quad (7)$$

where  $m$  is the mass and  $\vec{a}$  is the acceleration. Knowing  $\vec{a} = \frac{d\vec{v}}{dt} = \frac{d^2\vec{x}}{dt^2}$ ,  $q = -e$  (charge of an electron), and  $m = m_e$  (mass of an electron), Equation 7 becomes

$$-e\vec{E} = m_e \frac{d^2\vec{x}}{dt^2} \quad (8)$$

where  $\vec{x}$  is the position and  $t$  is the time. The initial conditions we defined earlier for the particle trajectories are needed to solve this 2<sup>nd</sup> order ordinary differential equation. Equation 8 has the same form in the  $y$  and  $z$  dimensions and so all three equations need to be solved in order to determine the three dimensional particle trajectory.<sup>3</sup>

Figure 20 shows a sample simulation of the electron trajectories in our setup. The detector potential is +200 V and the electrons have energies of 50 eV. 13 electrons were flown, having elevation angles from 0° to 120° degrees in steps of 10°. The particles are immediately affected by the electric field so that their initial direction angles are not obvious from the image

below. In Figure 20, some of the electrons strike the detector, i.e., they are collected, while some of the electrons miss the detector and instead strike the chamber.

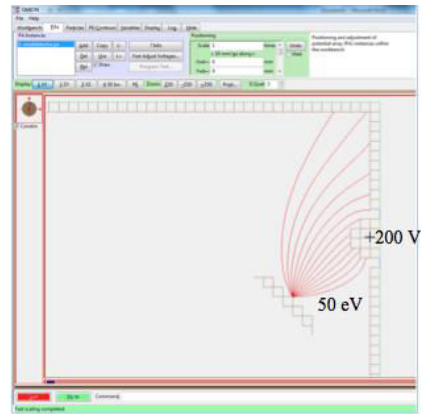


Figure 20: SIMION sample simulation.

If you want to visualize the influence of the electric field on the particle trajectory, you can select the PE/Contours tab at the top of the workbench screen and then select “PE View” to open the potential energy view (Figure 21). This view uses a three dimensional system where the x and y dimensions are position and the z dimension is potential energy. It makes it easier to see the varying potential map through the use of contours. The potential energy is highest by the detector and so the electrons want to travel uphill to the detector.

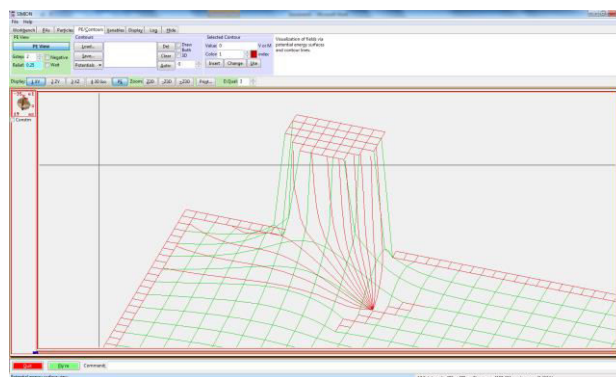


Figure 21: SIMION PE View.

## **RESULTS AND DISCUSSION**

Data obtained from the CASINO modeling program is presented first in this section. Data obtained from the SIMION modeling program is presented second in this section. The last part of this section describes our novel system design to improve the secondary electron collection efficiency of the detector.



## CASINO Data

For all of the simulations done in CASINO, a beam energy of 10 keV was used. The scans were all done on the (0, 0, 0) point. The beam diameter and spacing were both selected to be 10 nm. The option to generate secondary electrons was selected. For advanced settings, a beam semi-angle of 20 milliradians was used. For the line scans that will be shown later in this section, the beam diameter and spacing were both 10 nm and the line was scanned from the – 3100 nm point to the +3100 nm point on the x-axis and was at 0 along the y axis.

Although the initial goal of these simulations was to obtain data on secondary electron energies, directions, and spatial distributions to be used in the SIMION program, our group was unable to create a bridge to export this data from CASINO to SIMION. Even though this initial goal was not realized, very useful data was obtained using the CASINO program that could be useful when the bridge is made. Some of this data includes histograms of secondary yields and backscatter coefficients along with the standard deviation of these distributions. Using this data, statistical significance of the number of electrons simulated was analyzed.

Gold ( $Z = 79$ ) and tungsten ( $Z = 74$ ) were used as two different substrate materials in order to obtain statistical data to differentiate the two materials based on their yields. Using a gold block with dimensions of 10,000 nm x 10,000 nm x 3,000 nm, 100 simulations were done at the (0, 0, 0) point using 100 electrons, 1,000 electrons, and 10,000 electrons. During each of these 100 simulations, the resulting backscatter coefficient and secondary yield values were recorded. After the 100 simulations were completed, histograms of the data were created that allow us to interpret which values seem acceptable and which values seem to be outliers. In Figure 22, histograms of the backscatter and secondary yields were created for the gold substrate

using 100 electrons in the simulation. As shown in Figure 22, the values have a vast range. This is not sufficient for simulations moving forward. Figure 23 shows the same types of histograms, but for a tungsten block instead of a gold block. When comparing Figures 22 and 23, it is hard to differentiate between which material is gold and which material is tungsten because the distributions are too similar. There is too much variation in the values because of the large range and it does not seem that proper statistical data can be created from simulations using 100 electrons. This means that in order to continue to determine the proper amount of electrons needed to have reliable statistical data, more electrons need to be used.

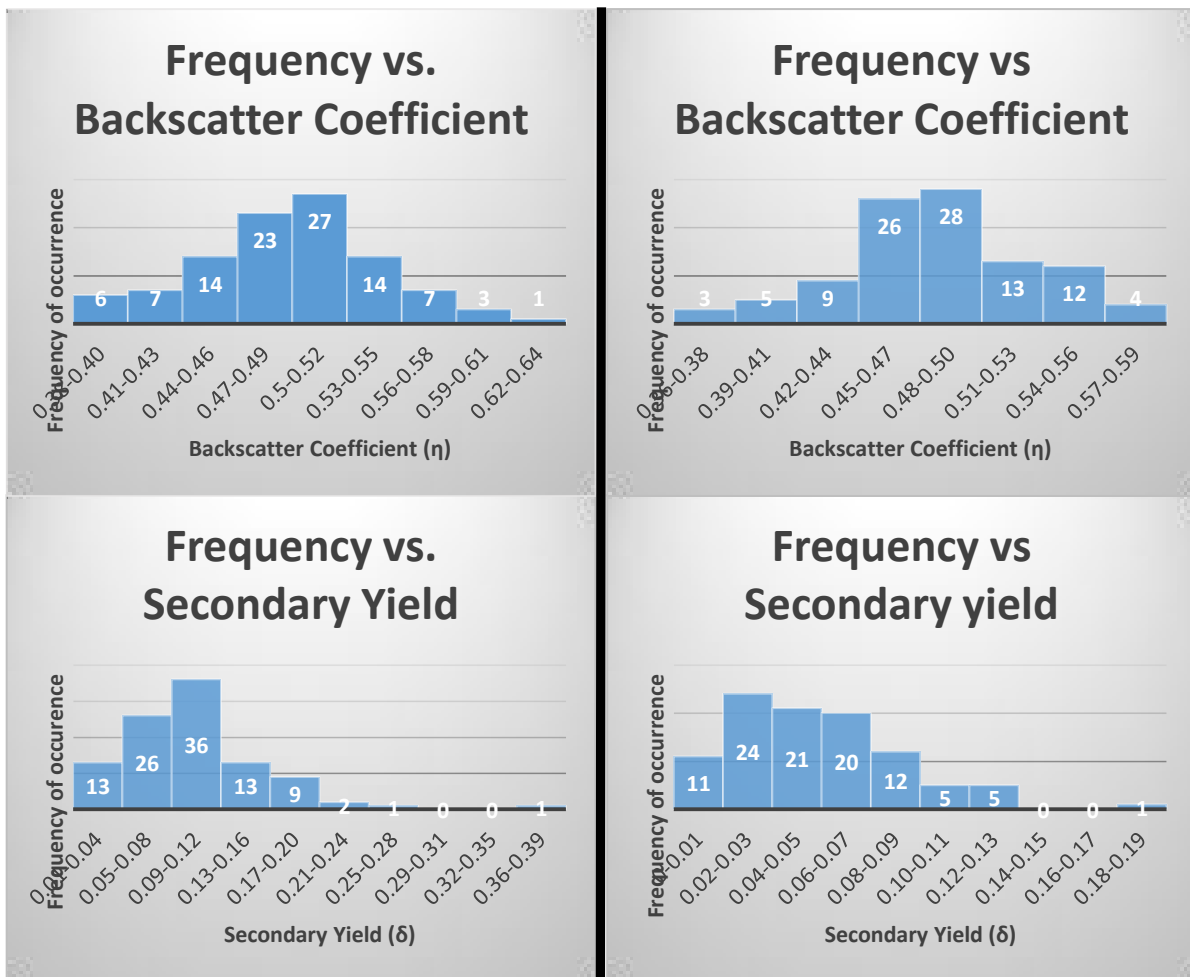


Figure 22: Distribution of yields for gold substrate for simulations using 100 electrons. Figure 23: Distribution of yields for tungsten substrate for simulations using 100 electrons.

The next set of simulations were done using all of the same conditions as used in the previous ones; however, 1,000 electrons were used instead of 100 electrons. When simulations are done using 1,000 electrons, there is a much tighter distribution in comparison to the simulations done using 100 electrons. It is seen that the range of values for backscatter distribution in gold is 0.26 for the simulations using 100 electrons while the range of the backscatter distribution in gold using 1,000 electrons is 0.072. Obviously, this range is much more concise and shows that as more electrons are added to the simulation, the distribution of the coefficients gets much tighter. This same trend is shown for the secondary yield values. When 100 electrons are used in the gold simulation, the range of the values is about 0.27 while the range for 1,000 electrons is 0.099. This is another drastic decrease in the range that gives us a much tighter distribution. The same type of trend is noticed for the tungsten simulations. In Figure 25, the distribution data for tungsten using a simulation of 1,000 electrons is shown. When comparing this to Figure 24, it is seen that there is starting to be a distinct difference in the distributions between gold and tungsten. For example, the average high value for the secondary yield in gold is approximately 0.11. When looking at the tungsten average high value for the secondary yield, the number is more close to 0.05. This is very important for analysis of information because when using 1,000 electrons, the difference in the materials makes itself much clearer than when only 100 electrons were used. Although 1,000 electrons seems to give us a much tighter and better distribution of data, our group was curious as to whether this amount of electrons used in simulations is truly enough.

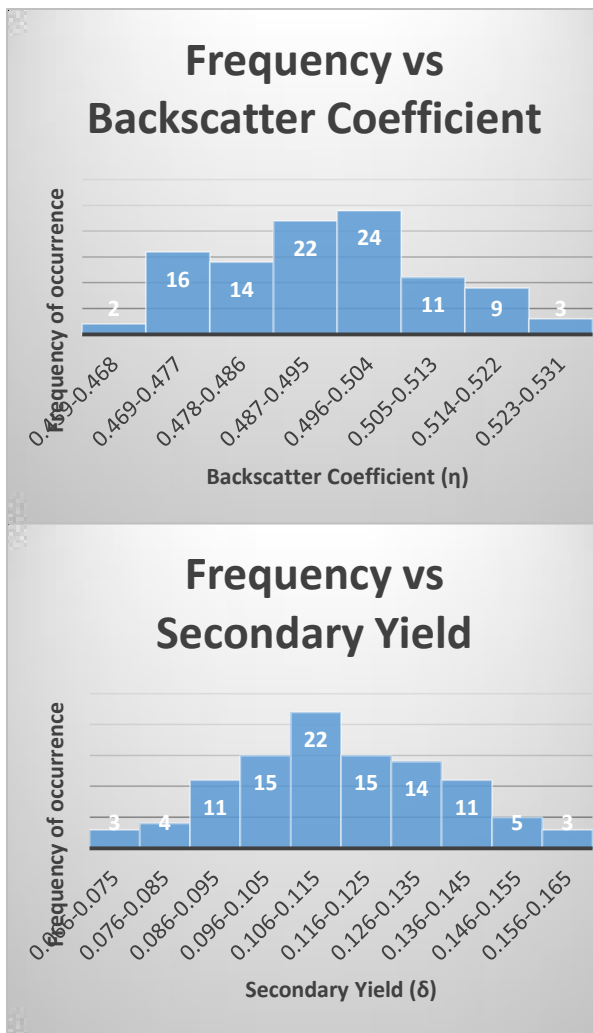


Figure 24: Distribution of yields for gold substrate for simulations using 1,000 electrons.

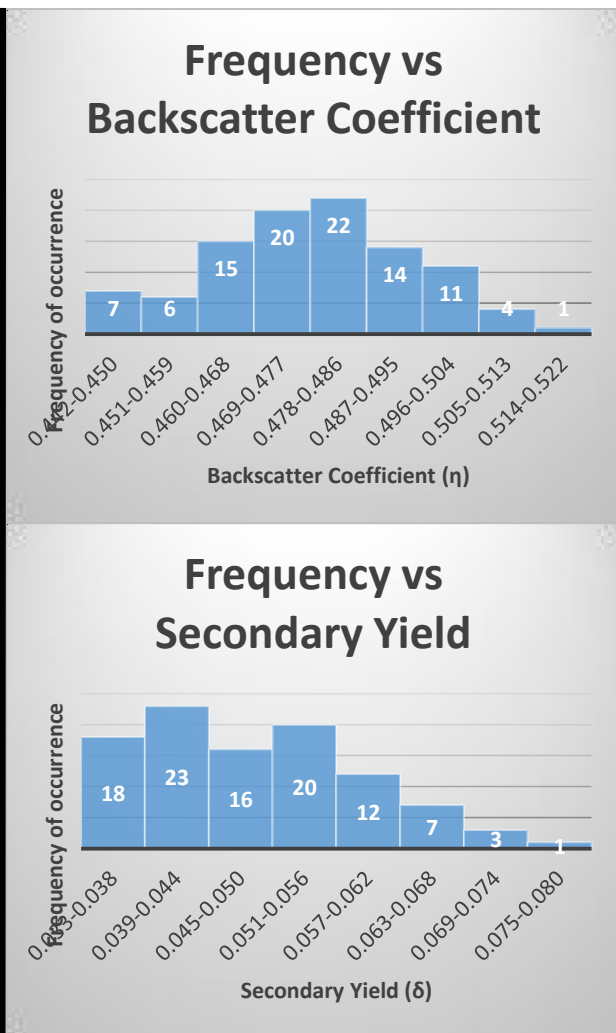


Figure 25: Distribution of yields for tungsten substrate for simulations using 1,000 electrons.

Therefore, the next step that was taken was to use 10,000 electrons in our simulations, which is another order of magnitude higher than the 1,000 electron simulations. So, once again, 100 simulations were ran on the gold and tungsten blocks with 10,000 electrons being used in the simulation (all other factors remained the same as in the previous simulations). Figure 26 shows the data for the gold block distribution for 100 simulations using 10,000 electrons. In these histograms, there is an even tighter range than the simulations that were using 1,000 electrons.

The range here is 0.0278 for the backscatter coefficient and is 0.0368 for the secondary yield. It is also very important to point out that as more electrons are simulated, the number given for the yields will have an additional decimal place of accuracy. For 100 electrons, the accuracy was to 2 decimal places, for 1,000 electrons, the accuracy was to 3 decimal places, and finally, for 10,000 electrons, the accuracy is to 4 decimal places. This trend will continue as more electrons are simulated such as 100,000 or one million. Our ability to do simulations with 100,000 or one million electrons was limited by time to complete these simulations and computing power of the machines that were used to carry out the simulations.

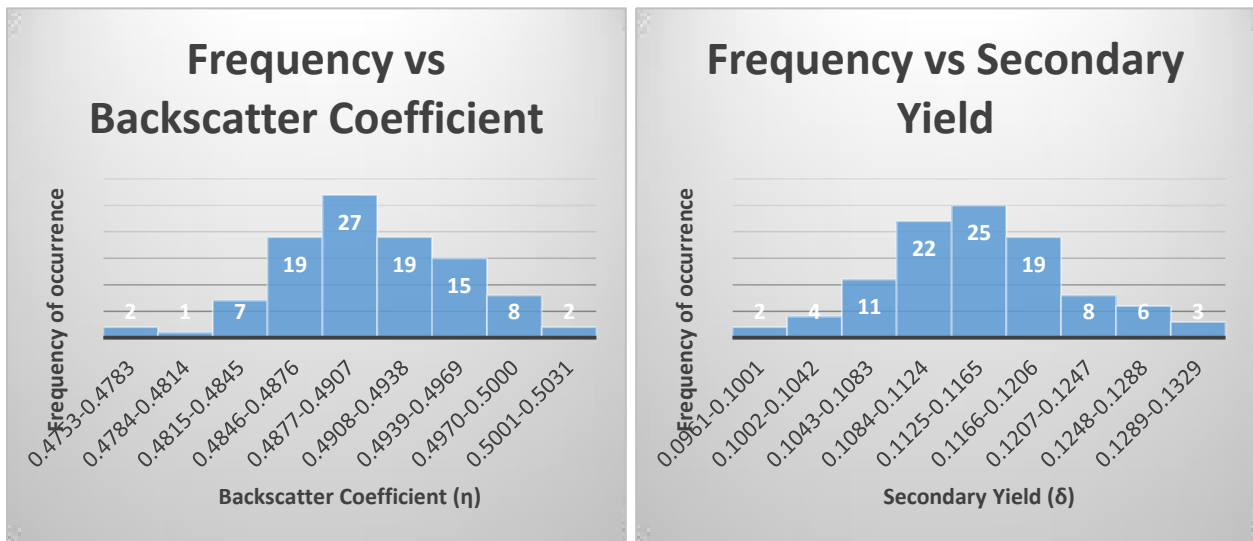


Figure 26: Distribution of yields for gold substrate using simulations of 10,000 electrons.

The next and final set of histograms represented in Figure 27 show the simulations of 10,000 electrons on the tungsten substrate instead of the gold. Figures 26 and 27 represent the most significant and accurate data that was obtained from all of the simulations. First, when looking at the average high value for the backscatter coefficient in gold, a value of approximately 0.49 is obtained. This is a high value for the backscatter coefficient; however, it makes a lot of

sense due to the Z contrast of backscatter coefficient. This Z contrast relation basically states that as the number of the element on the periodic table increases, the backscatter coefficient will increase. Thus, it is expected to be lower for elements such as carbon while it is very high (almost max) for gold and tungsten. Based on Z contrast, tungsten should have a slightly lower backscatter coefficient than gold. When looking at the average high value for the backscatter coefficient in tungsten, a value of approximately 0.48 is obtained. As expected, this value is lower than gold; but, it is only slightly lower. This means that it may be more difficult to come up with a model of what value of backscatter coefficient would correlate to either tungsten or gold. Something in which a significant difference in value is seen is in terms of the secondary yields. The average high value for the gold block in terms of the secondary yield is approximately 0.1148. For tungsten, this value is approximately 0.0503. This allows a more clear decipher between which value of secondary yield will correlate to gold or tungsten.

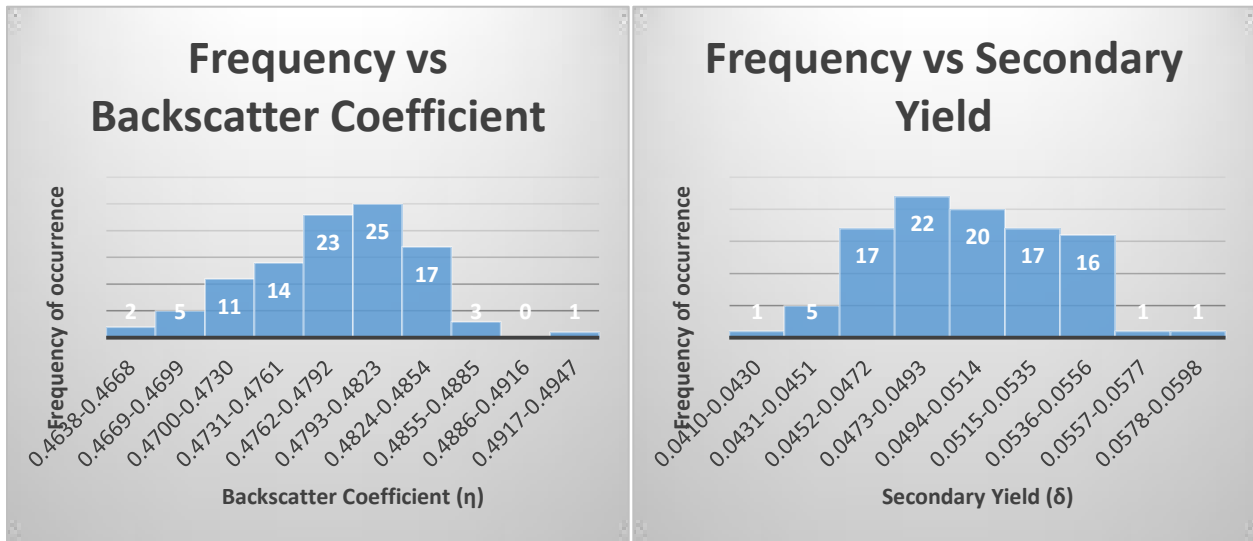


Figure 27: Distribution of yields for tungsten substrate for simulations using 10,000 electrons.

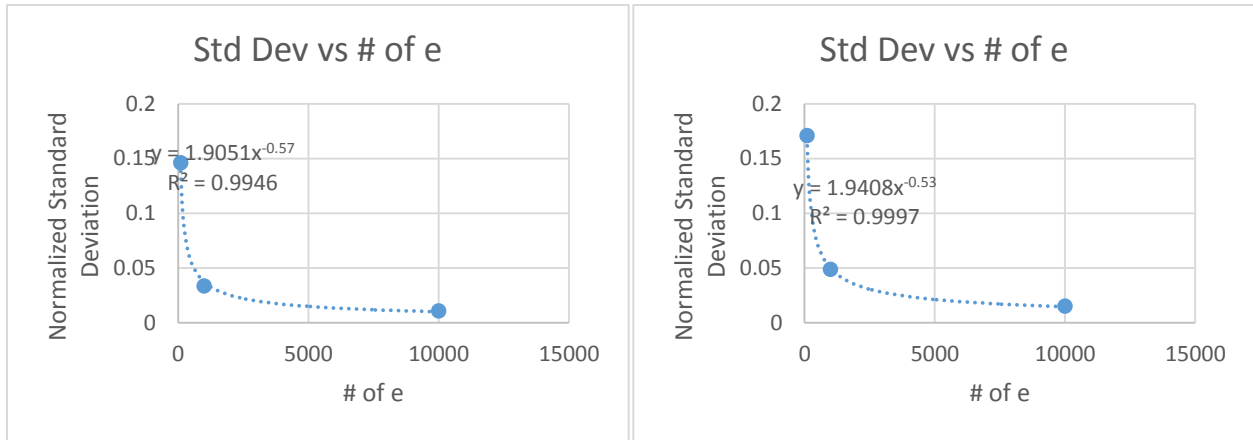


Figure 28: Plots of normalized standard deviation as a function of the number of electrons used in the simulation. The graph on the left is normalized to the average backscatter coefficient while the graph on the right is normalized to the average secondary yield.

Figure 28 shows two graphs of normalized standard deviation as a function of the number of electrons simulated. Out of the 100 simulations ran for 100, 1,000, and 10,000 electrons, a standard deviation of the 100 values obtained for the yields of each respective number of electrons was calculated. This is very closely related to the accuracy and range of the histograms shown previously. The standard deviation of the values for 100 electrons is a large number compared to the other two cases. This is because the range of values is so high and scattered when using this small number of electrons that good statistical data is likely not to result from simulations using only 100 electrons. There is a drastic drop off in standard deviation moving from 100 to 1,000 electrons. This is related to the range of the simulations using 1,000 electrons being much smaller than the simulations using 100. When comparing this further to 10,000 electrons, the trend seems to level off as it heads from 1,000 to 10,000 electrons. Relating it to the change in range discussed above, the drop off from 1,000 to 10,000 was much less drastic than 100 to 1,000 electrons, which further helps to validate this data. Although the change in deviation from 1,000 to 10,000 electrons does not seem like a lot, it is still greater than the

change when going from 10,000 to 100,000 electrons. The difference in deviation between 1,000 and 10,000 electrons is 0.0227. Using the equation on the graph in Figure 28, the deviation for 100,000 electrons can be predicted. The difference in deviation between 10,000 and 100,000 electrons is 0.0079. From this, it is clear that using 1,000 electrons may be sufficient enough in certain application, but, it would be much better to use at least 10,000 electrons moving forward.

In order to determine whether a secondary yield value will correlate to tungsten or gold, a standard  $2\sigma$  deviation will be used. Also, to give the most accurate statistical data, the numbers obtained from the simulations using 10,000 electrons will be used. The average of the yield values for gold is 0.1148 as shown above. The standard deviation for this set of numbers is given by 0.00744. Multiplying this by two will give us the proper spread:

$$2\sigma_{\text{gold}} = 0.014879 \quad (9)$$

Using this  $2\sigma$  value, the upper and lower limits of acceptable values for secondary yields in gold can be determined. The lower limit is represented by Equation 10 while the upper limit is represented by Equation 11:

$$0.1148 - 2\sigma = 0.0999 \quad (10)$$

$$0.1148 + 2\sigma = 0.1297 \quad (11)$$

Based on Equations 10 and 11, it can be concluded that the range of acceptable values for the secondary yield in gold will fall between 0.0999 and 0.1297. Anything outside of this range will result in outliers that can skew other types of statistical data. Moving on to tungsten, the average of the yield values when using 10,000 electrons is 0.0503. The standard deviation for this set of numbers is given by 0.003607. Using the same method above, multiplying by 2 will give us our proper spread:

$$2\sigma_{\text{tungsten}} = 0.007214 \quad (12)$$



The lower and upper limits for the tungsten are represented by Equations 13 and 14, respectively:

$$0.0503 - 2\sigma = 0.0431 \quad (13)$$

$$0.0503 + 2\sigma = 0.0575 \quad (14)$$

Using Equations 13 and 14, the acceptable range for secondary yield values in tungsten falls between 0.0431 and 0.0575. Using these two ranges can help to differentiate between the two materials. For example, if a substrate is made of half gold and half tungsten, then by doing a line scan and looking at the yield obtained, one will be able to clearly say which half is gold, which half is tungsten, and at what point the boundary is located. This example leads into the next set of data that more clearly shows the significance of the number of electrons used in a scan.

Very similar to what was just described above, a simple half gold and half tungsten block was created. A line scan consisting of approximately 600 different points was done from the tungsten half to the gold half of the block. This line scan was done 3 times: the first scan was done using a beam of 100 electrons, the second scan was done using a beam of 1,000 electrons, and finally, the third scan was done using a beam of 10,000 electrons. It is important to keep in mind the significance of the amount of electrons in a simulation shown above when looking at these next couple of figures.

Starting off by looking at Figure 29, it is seen that the position of the scan has negative values and positive values. For this instance, the negative numbers are the tungsten half of the block while the positive numbers correlate to the gold part of the block. The 0 point is the boundary between the two different materials. On the y axis, the secondary yield values that were obtained are multiplied by 100 since 100 electrons were used. Although there is a slight difference between the secondary yields between the tungsten half and the gold half, the data is overall too sporadic and doesn't necessarily show a trend. As it is known, the difference between

the yield values of gold and tungsten should be clearly distinguishable; yet, this graph barely shows a difference between the two materials. Thus, it further helps to prove that simulations using 100 electrons do not provide the user with significant data. It is clear that in order to obtain better data, more electrons need to be used.

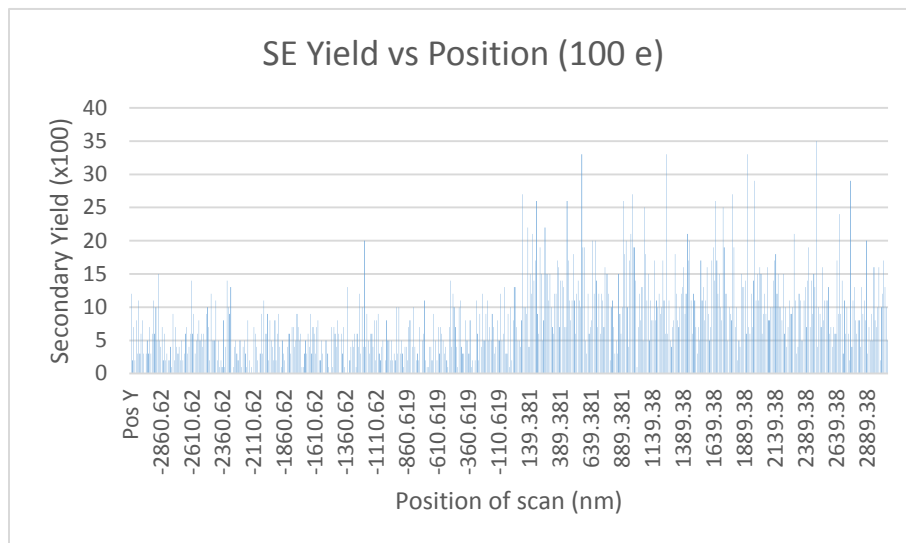


Figure 29: Line scan of secondary yield vs. position on the block using 100 electrons.

In Figure 30, the same line scan was done with an electron beam consisting of 1,000 electrons instead of 100. When looking at this graph, the trend in data is much more distinct than that shown in Figure 29. It is as if one would almost be able to draw a flat average line across the two different halves to give two distinct average yield values. The only slight problem with this set of data may be that the user is looking for even more accurate results. Even though there is somewhat of a difference in height (yield value) between the two materials, the values for secondary yield have a range that might be larger than someone would feel comfortable with. This further goes back into a point mentioned previously saying that 1,000 electron simulations

may be acceptable to some users; however, many users would probably want data they can be fully content with. Using 10,000 electrons in the simulation may provide a level of comfort with the data.

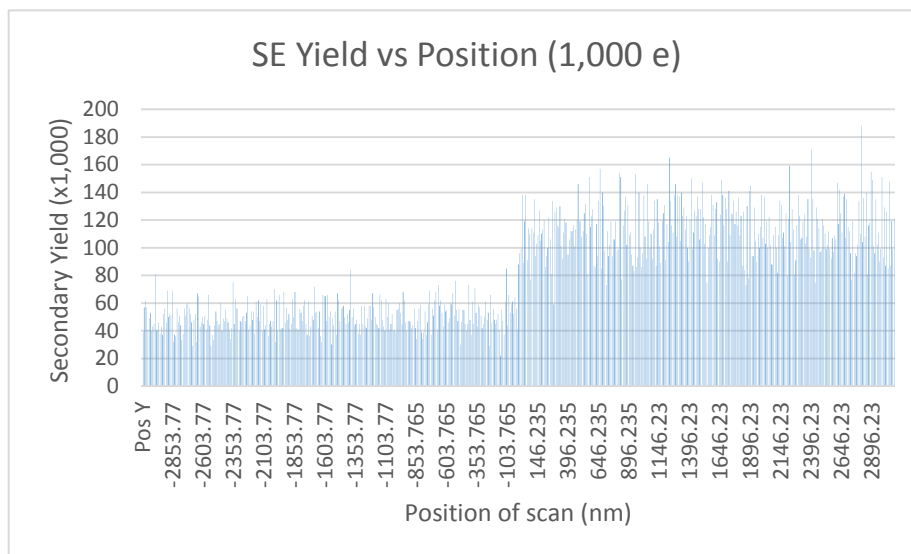


Figure 30: Line scan of secondary yield vs. position on the block using 1,000 electrons.

Figure 31 shows the same line scan done previously but now uses 10,000 electrons in the beam. This graph provides us with an extremely precise set of data. There is an observable difference between the two halves of the block. Discussed above, the average value for secondary yield in tungsten is around 0.0503. When looking at the negative positions, almost all of the values are close to 0.05. The variation is very miniscule and based on the statistical distribution calculated above, it is likely that most of these values would be accepted as good values for secondary yield of tungsten. Moving on to the gold half, the secondary yield average value was approximately 0.1148. When looking at the positive values in Figure 31, it is clear that

most of the values are close to this while there may be a few outliers. Overall, most of these points would probably fall within the  $2\sigma$  standard deviation and be tallied as acceptable values.

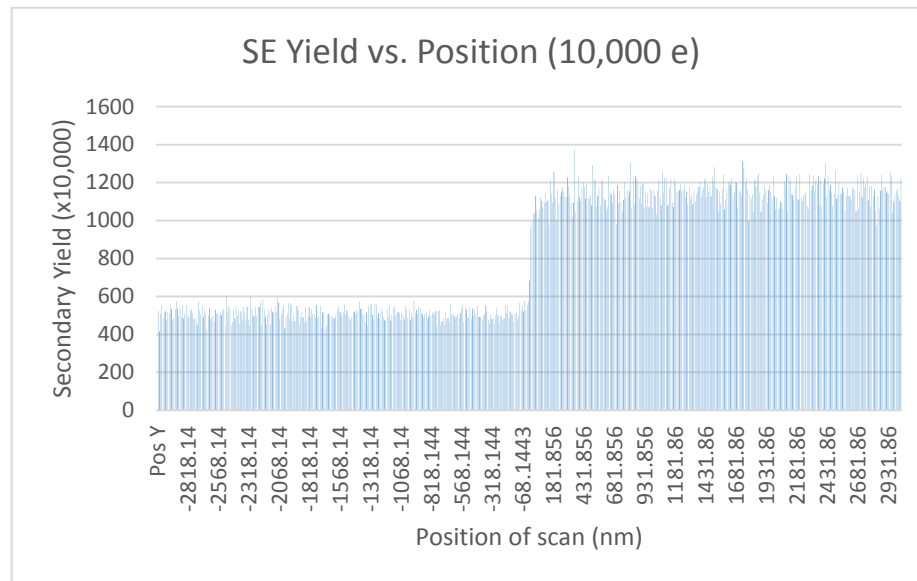


Figure 31: Line scan of secondary yield versus position on the block using 10,000 electrons.

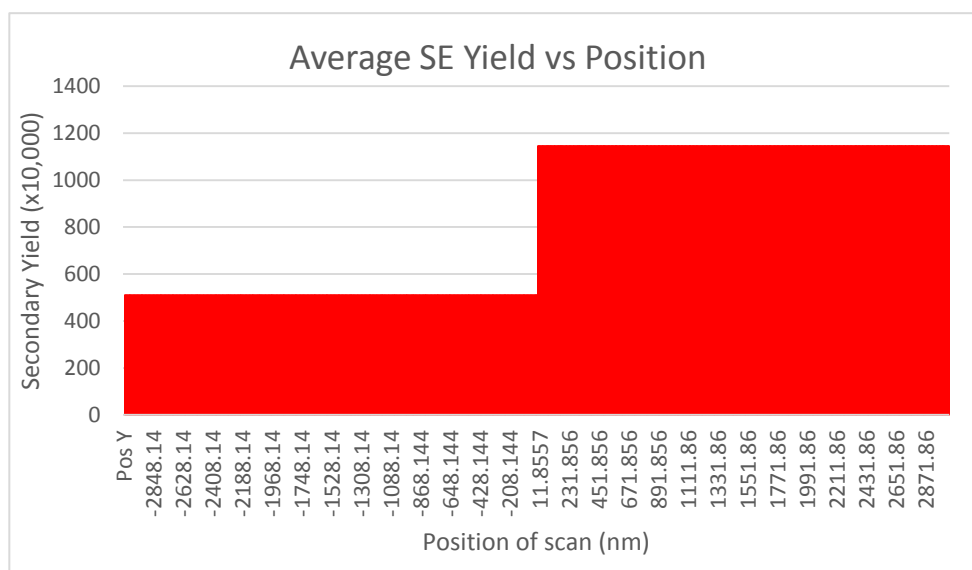


Figure 32: Line scan of average secondary yield vs. position using the data from the 10,000 electron scan.

One final piece of information to show before wrapping up the relationship between these three figures is shown in Figure 32. In figure 32, all of the secondary yield values from Figure 31 were averaged for the tungsten half and the gold half of the block. These two average value were plotted as the value for all of the points on the line scan corresponding to the tungsten and gold halves. Figure 32 can be thought of as a possible set of data for what might be obtained if a simulation of one million electrons was done. Moving from Figures 29 to 31, we see that the graphs become more distinct, the two halves are easily distinguishable from one another, and the range of the values significantly decreases. This in turn means that using a scan of one million or more electrons can give a graph similar to Figure 32 in which the range of the values is almost zero and actually just looks like one solid line of the same value.

## SIMION Data

Using our detector setup described in the “SIMION Modeling Program” section, trajectory simulations were obtained in order to evaluate the efficiency of secondary electron collection by the detector. The secondary electron collection efficiency ( $\gamma$ ) is the ratio of the number of secondary electrons collected by the detector to the number of secondary electrons emitted from the sample. For all of the 2D simulations, 13 electrons were flown, having elevation angles from  $0^\circ$  to  $120^\circ$  degrees in steps of  $10^\circ$ . The detector potential and the energies of the electrons are specified for each simulation.

Figure 33 shows a simulation demonstrating the collection of low-energy secondary electrons by the detector. The detector potential is +200 V and the electrons have energies of 5 eV. All of the 13 flown electrons were collected by the detector ( $\gamma = 100\%$ ). This shows that the current detector setup in an SEM is very efficient for collecting most secondary electrons emitted from the sample since most secondary electrons have low energies around 5 eV.

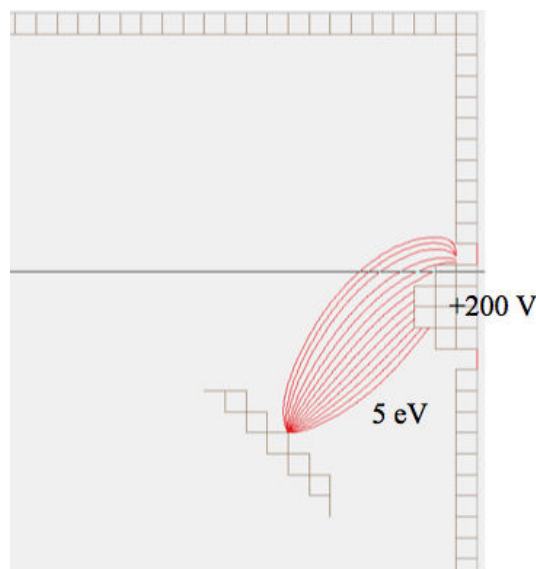


Figure 33: The collection of low-energy (5 eV) secondary electrons by the detector.

Since most low-energy secondary electrons are collected by the detector, we now investigate the collection efficiency of high-energy secondary electrons. Figure 34 shows a simulation (using the same detector setup as before) demonstrating the collection of high-energy secondary electrons by the detector. The detector potential is +200 V and the electrons have energies of 50 eV (which is the maximum cutoff energy for secondary electrons). Only 8 out of 13 flown electrons were collected by the detector ( $\gamma = 62\%$ ). This shows that the current detector setup in an SEM is not very efficient for collecting high-energy secondary electrons (close to 50 eV) emitted from the sample at high elevation angles. In this example, it will not collect secondary electrons with elevation angles greater than  $70^\circ$ . Although not shown in the image below, high-energy secondary electrons with elevation angles less than  $0^\circ$  may also miss the detector.

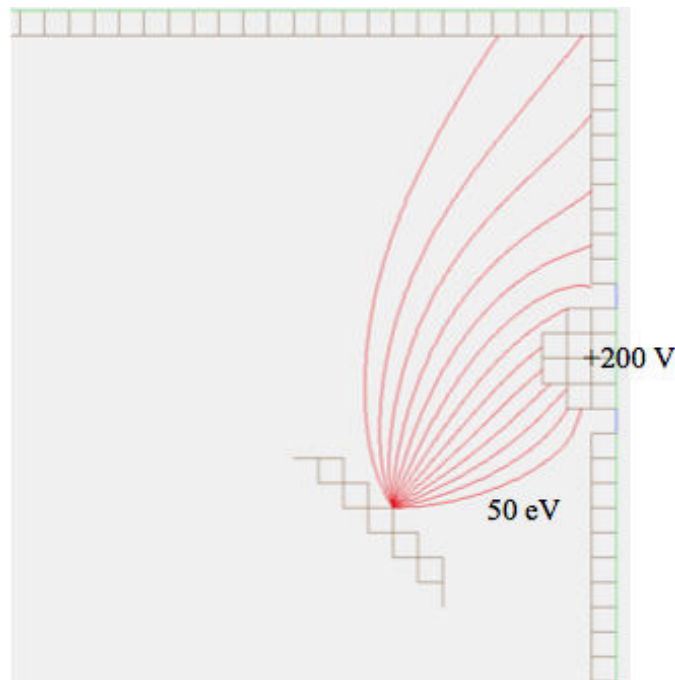


Figure 34: The collection of high-energy (50 eV) secondary electrons by the detector.

In the literature, typical values cited for the detector potential are +200 V, +300 V, and +400 V. Since the Everhart-Thornley detector can easily adjust its operating voltage, we are interested in determining which operating voltage is the optimal choice to apply to the detector. In Figure 35, we show two simulations for 50 eV secondary electrons with identical setups and operating parameters except for the detector potential: the detector in the left image has a potential of +200 V, while the detector in the right image has a potential of +400 V. It can be seen that the detector with the increased potential does not collect any additional secondary electrons, but the high elevation angle trajectories are attracted slightly closer to the detector by approximately  $5^\circ$ . Therefore, increasing the detector potential from +200 V to +400 V does not improve the collection efficiency drastically. However, although not shown in the images below, more high-energy secondary electrons with elevation angles less than  $0^\circ$  would likely be collected due to the stronger electric field near the bottom of the detector.

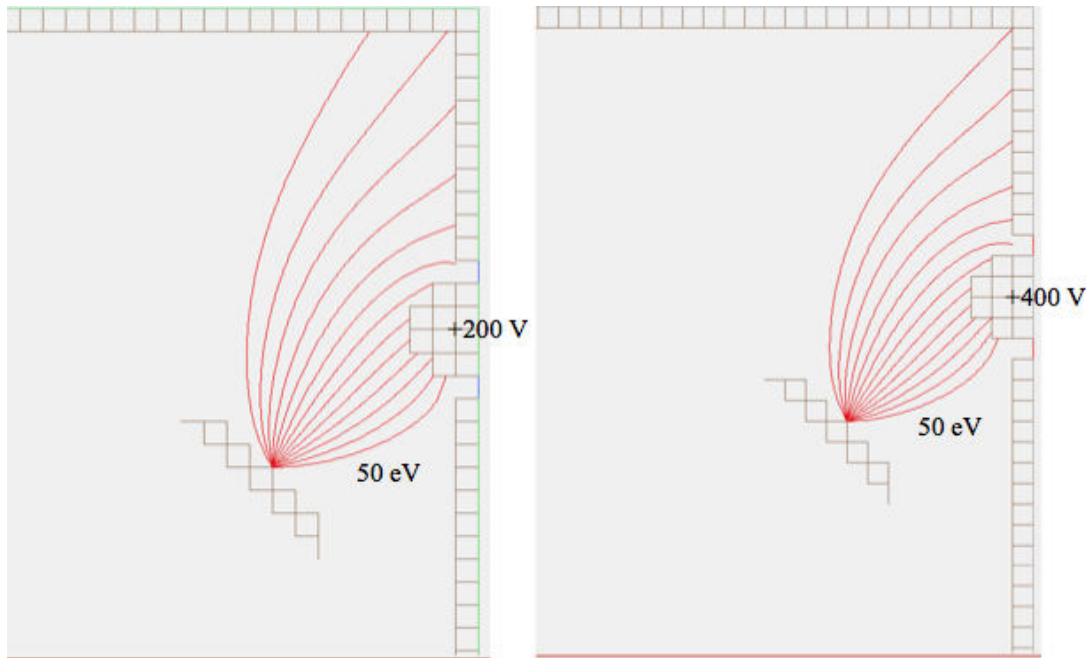


Figure 35: The effect of detector potential (left image: +200 V, right image: +400 V) on the collection of high-energy (50 eV) secondary electrons by the detector.



We next are interested in determining the effect of the detector size on the collection of high-energy (50 eV) secondary electrons by the detector. In Figure 36, we show two simulations with identical operating parameters (+200 V) and setups except for the detector size: the detector in the left image is 4 cm in diameter, while the detector in the right image is 8 cm in diameter. It can be seen that the detector with the increased size collects an additional secondary electron ( $\gamma = 69\%$ ), which is 7% greater than for the smaller detector ( $\gamma = 62\%$ ). Therefore, increasing the detector size from 4 cm to 8 cm slightly improves the collection efficiency, allowing for the collection of secondary electrons at angles  $10^\circ$  greater than before. Although not shown in the images below, more high-energy secondary electrons with elevation angles less than  $0^\circ$  would likely be collected due to the larger electric field near the bottom of the detector.

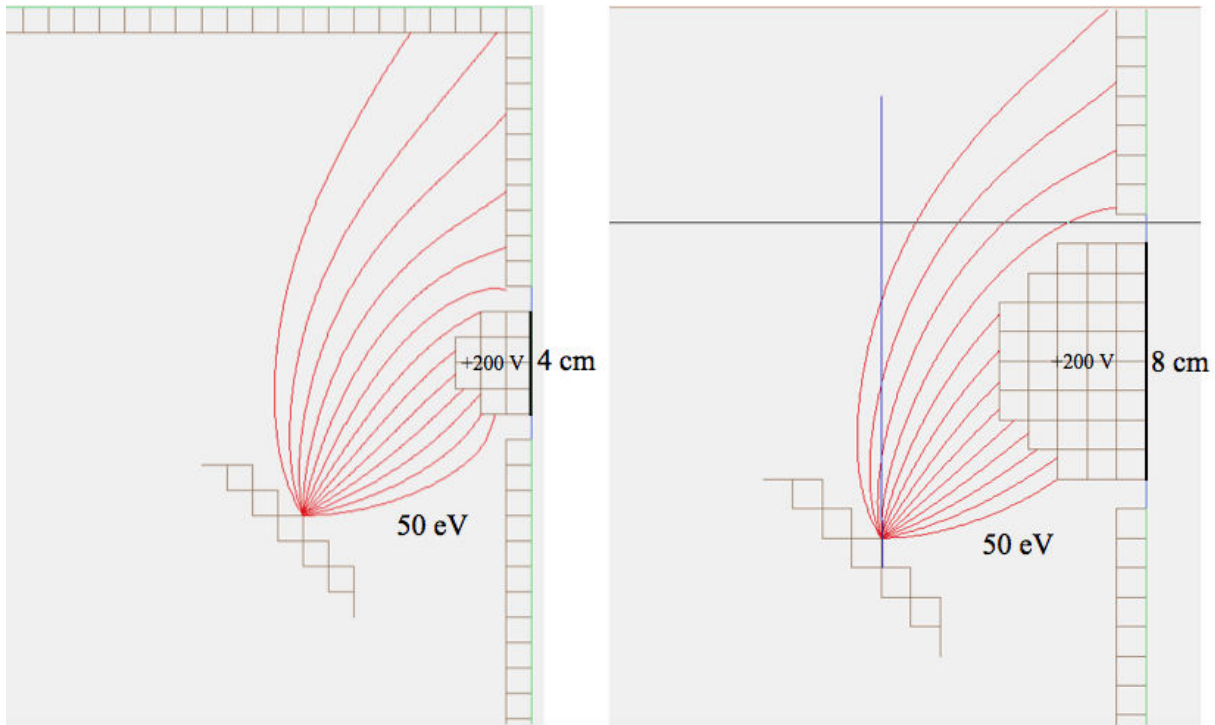


Figure 36: The effect of detector size (left image: 4 cm, right image: 8 cm) on the collection of high-energy (50 eV) secondary electrons by the detector.

Preliminary work was done using a 3D model, which more accurately imitates the environment inside an SEM: a grounded, cubic chamber; a grounded, inclined plane sample holder; and a hemispherical, electrically biased control grid (which acts as the detector). Figure 37 shows a sample simulation using our 3D model. In this setup, the detector potential is +200 V and the electrons have energies of 10 eV. 13 electrons were flown, all having a constant  $45^\circ$  elevation angle and an azimuth angle ranging from  $0^\circ$  to  $120^\circ$  degrees in steps of  $10^\circ$ . As expected, all of these low-energy secondary electrons were collected. The 3D model is much more complex to design but it is a more accurate model of the detector setup in an SEM. In the 3D model, there are many more combinations of possible electron trajectories than the 2D model due to having an azimuth angle in addition to the elevation angle. It can be very time-consuming inputting the initial conditions of many particles now that more direction angles are available. More work needs to be done to repeat our experiments from our 2D model in our 3D model.

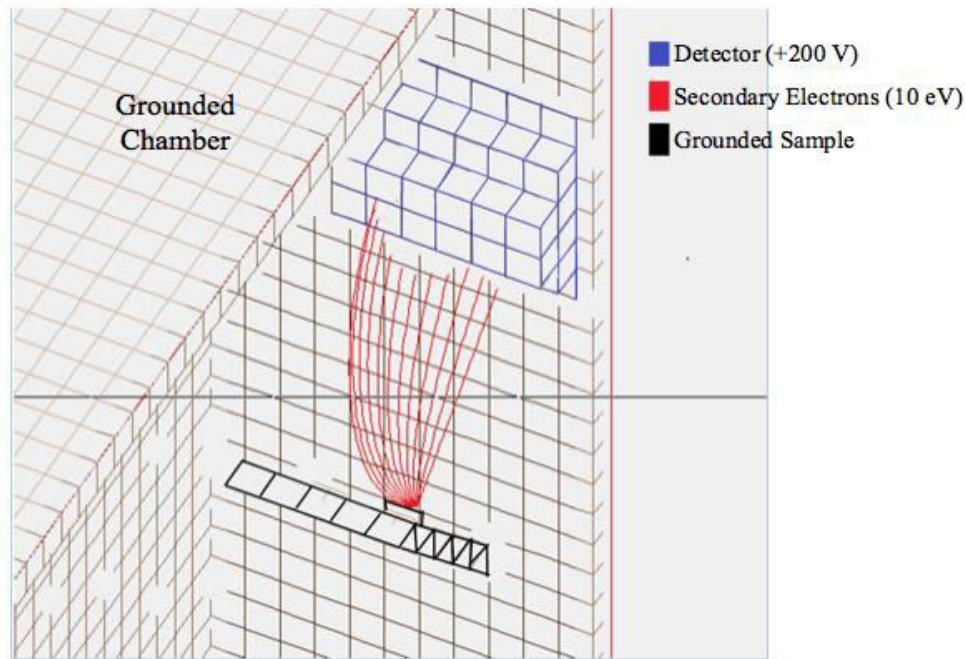


Figure 37: SIMION sample simulation using a 3D model.

## Our Improved System Design

In the current secondary electron detector setup of an SEM, not all of the secondary electrons emitted from the sample are collected by the detector (Figure 38). Many high-energy secondary electrons (close to 50 eV) emitted from the sample at high elevation angles as well as at steep downward trajectories are not collected by the detector. Even though only a small amount of the emitted secondary electrons have high-energy, the ability of the Everhart-Thornley detector to collect these high-energy secondary electrons will maximize its collection efficiency.

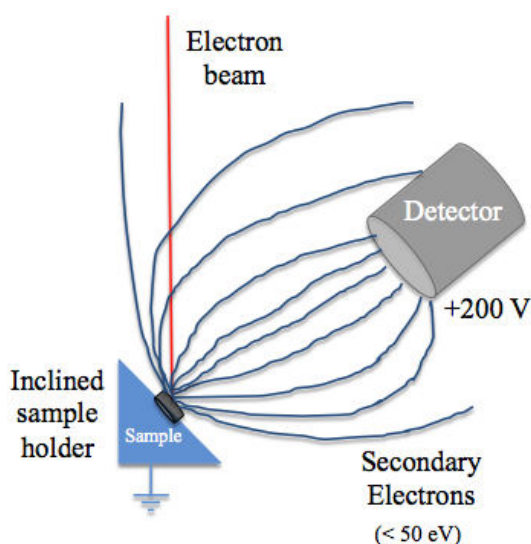


Figure 38: Current detector setup.

Figure 39 shows our improved system design using a side pusher electrode. This electrode has a potential of  $-200$  V, which allows it to repel the high-energy secondary electrons with high elevation angles towards the detector. In our setup with the pusher electrode, more secondary electrons can be collected by the detector, thus enhancing the signal-to-noise ratio. Note that the small voltage of the pusher electrode ( $-200$  V) does not affect the high-energy

electron beam (20 keV). This should be evident from the fact that the small voltage of the detector (+200 V) also does not affect the electron beam and both of the electrodes are at similar distances from the incident beam.

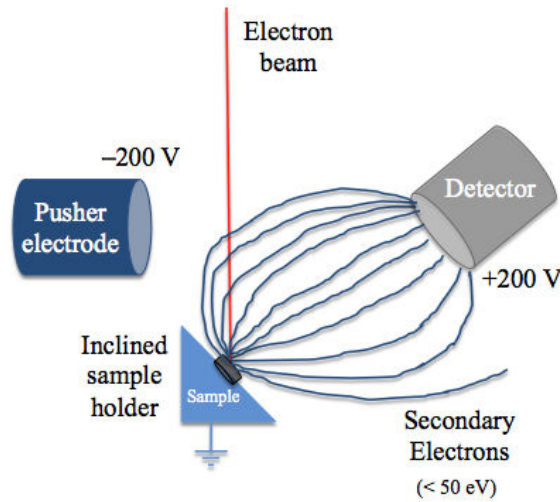


Figure 39: Improved system design using a side pusher electrode.

Figure 40 shows a SIMION model of our improved system design. While the current detector setup collects 8 out of 13 flown electrons ( $\gamma = 62\%$ ), our setup collects 12 out of 13 flown electrons ( $\gamma = 92\%$ ), which is 30% greater than the current detector setup. While the current detector setup can collect electrons up to  $70^\circ$ , our setup can collect electrons up to  $120^\circ$ , which is  $50^\circ$  greater than the current detector setup. Our setup shows a dramatic improvement in collection efficiency. The PE View of the pusher electrode setup shows that the side pusher electrode makes it easier for secondary electrons at higher elevation angles to travel uphill to the detector by increasing the electric field in the area above and to the left of the sample holder (Figure 41). The lower electron that missed the detector in our setup but not the current detector setup likely resulted from the pusher electrode being too close to the sample, causing the electron

to stay at its low trajectory ( $0^\circ$ ) a bit longer so that it was not as strongly influenced by the detector potential. To avoid this, the pusher electrode should be slightly raised.

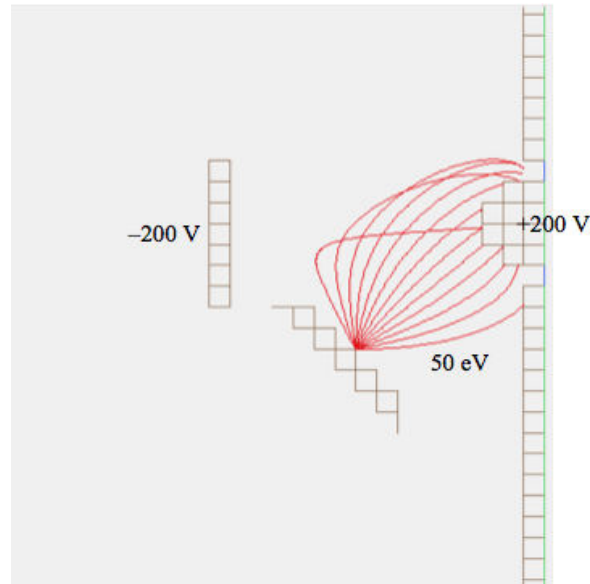


Figure 40: SIMION model of our improved system design.

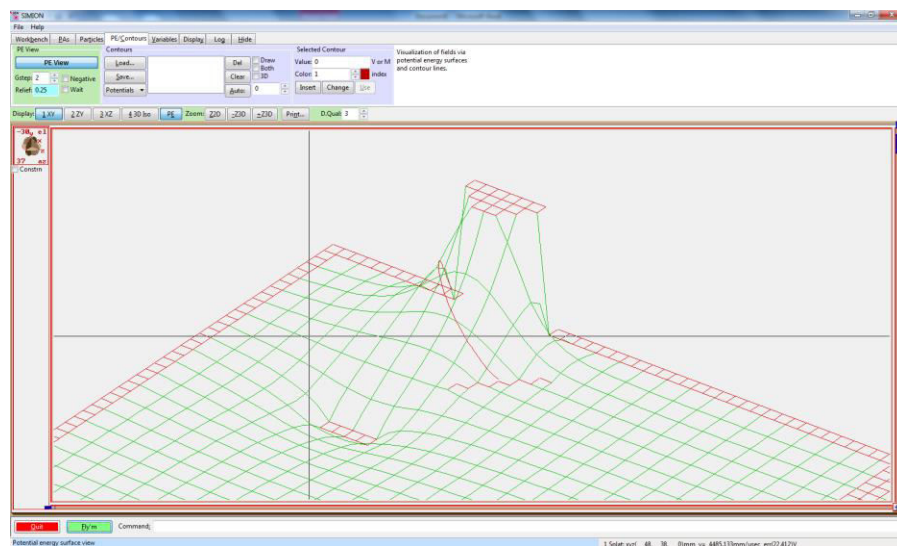


Figure 41: PE View of pusher electrode setup.

By increasing the detector potential from +200 V to +300 V, the electron with the low trajectory ( $0^\circ$ ) in Figure 40 is now collected (Figure 42). This improves the collection efficiency to 100%. It also demonstrates that increasing the detector potential may help collect secondary electrons with slight downward trajectories due to the larger electric field near the bottom of the detector. A solution to capture secondary electrons with steep downward trajectories is to use a bottom pusher electrode (Figure 43). This may not be as important as the side pusher electrode because less electrons miss at the bottom of the sample than at the top of the sample, but it can be used for very efficient systems to collect the most possible secondary electrons. Future work will focus on modeling secondary electrons with steep downward trajectories and validating the effectiveness of the bottom pusher electrode.

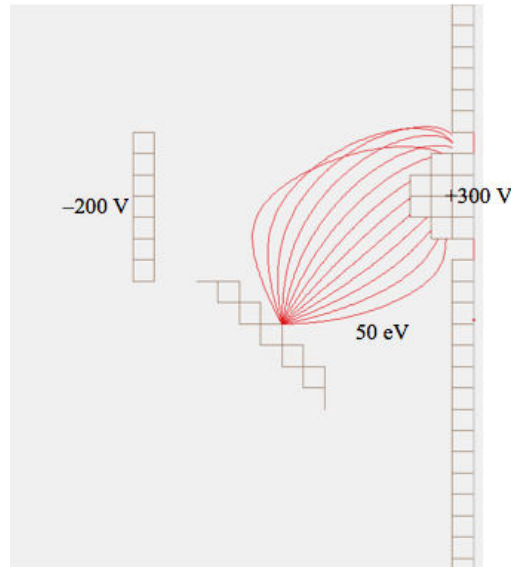


Figure 42: SIMION model of our improved system design using higher detector potential (+300 V).

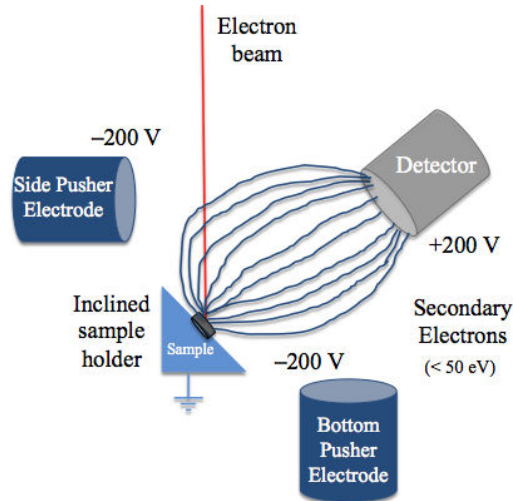


Figure 43: Improved system design using a side pusher electrode and a bottom pusher electrode.

Literature searches were conducted to determine if our improved system design with the pusher electrodes has been done before. The only literature we have found on using additional electrodes in an SEM is the Banbury-Dixon detector setup (published in 1969), which uses two electrodes added to the traditional SEM detector setup (Figure 44).<sup>8</sup> It uses a very different setup than our design. It consists of traditional electrode control grid by the detector (like in the Everhart-Thornley detector), but it uses a horizontal sample holder (rather than inclined) with an annular electrode surrounding it and another electrode on the side very similar to our side pusher electrode. However, the Banbury-Dixon detector setup was used to develop a new, directionally sensitive contrast mechanism based on varying the three electrode potentials instead of using the electrodes to collect more secondary electrons. Therefore, our system design seems to be novel.

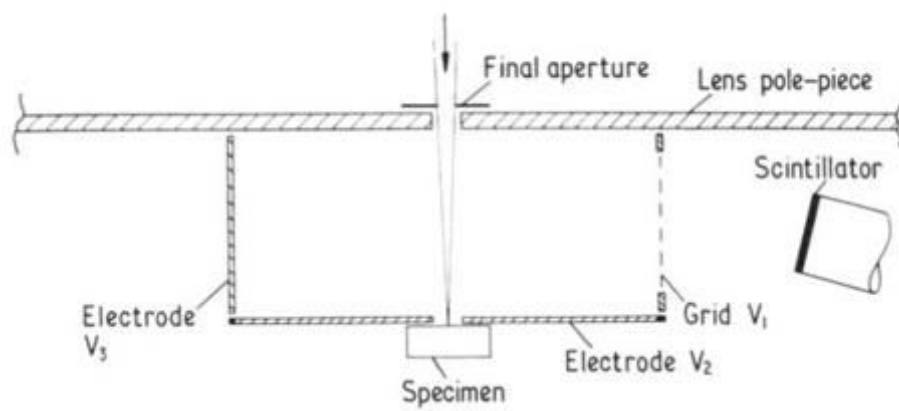


Figure 44: Banbury-Dixon detector setup.



## CONCLUSION

The CASINO work has shown that the number of electrons used in a simulation has a colossal effect on the accuracy of the data. The use of less electrons results in data with almost no statistical significance while using a lot of electrons will give data with great statistical significance. In general, as the number of electrons simulated increases, the data obtained becomes more accurate and reliable. In order to obtain significant statistical data from a Monte Carlo simulation, 10,000 electrons or more need to be used. The use of less than 10,000 electrons produces unreliable data.

SIMION has been used to successfully model the collection efficiency of the current detector setup in an SEM. While the Everhart-Thornley detector is very efficient because it collects most low-energy secondary electrons (which constitutes for the majority of the electrons emitted from the sample), it is not very efficient at collecting high-energy electrons. Increasing the detector potential from +200 V to +400 V does not drastically improve the collection efficiency of high-energy secondary electrons. In order to maximize the detector collection efficiency, a new system design was proposed to collect the high-energy secondary electrons. Through trajectory modeling using SIMION, our novel system design using a pusher electrode has to shown to greatly improve the collection of high-energy secondary electrons emitted from the sample at high elevation angles. Our goal of designing a more efficient detector setup to enhance the signal-to-noise ratio has been achieved.

## **FUTURE WORK**

Future work needs to be done to find a way to input the emitted secondary electron initial trajectory data from CASINO into SIMION for more accurate trajectory simulations. SIMION simulations need to be done to model secondary electrons with steep downward trajectories and validate the effectiveness of the bottom pusher electrode. More work needs to be done to repeat all of our experiments from the 2D model in the 3D model, especially measuring the improvement in secondary electron collection efficiency of the pusher electrode designs in the 3D model.

## REFERENCES

- [1] Goodhew, Peter J., John Humphreys, and Richard Beanland. *Electron microscopy and analysis*. CRC Press, 2000.
- [2] Vernon-Parry, K. D. "Scanning electron microscopy: an introduction." *III-Vs Review* 13.4 (2000): 40-44.
- [3] Reimer, Ludwig. "Scanning electron microscopy: physics of image formation and microanalysis." (2000): 1826.
- [4] Hafner, Bob. "Scanning electron microscopy primer." *Characterization Facility, University of Minnesota-Twin Cities* (2007): 1-29.
- [5] Seiler, H. "Secondary electron emission in the scanning electron microscope." *Journal of Applied Physics* 54.11 (1983): R1-R18.
- [6] Drouin, Dominique, et al. "CASINO V2. 42—A Fast and Easy- to- use Modeling Tool for Scanning Electron Microscopy and Microanalysis Users." *Scanning* 29.3 (2007): 92-101.
- [7] Demers, Hendrix, et al. "Three- dimensional electron microscopy simulation with the CASINO Monte Carlo software." *Scanning* 33.3 (2011): 135-146.
- [8] Banbury, J. R., and W. C. Nixon. "A high-contrast directional detector for the scanning electron microscope." *Journal of Physics E: Scientific Instruments* 2.12 (1969): 1055.